Master's Thesis of Engineering

Parametric Study on the Design Methodology of Post-Tensioned Nuclear Containments with High Performance Concrete

고성능 콘크리트를 적용한 포스트텐션 원전 격납건물의 설계방법론에 대한 매개변수 연구

August 2022

Graduate School of Engineering

Seoul National University

Architecture and Architectural Engineering

Seung Heon Lee

Parametric Study on the Design Methodology of Post-Tensioned Nuclear Containments with High Performance Concrete

Advisor: Thomas Kang

Submitting a Master's thesis of
Architecture and Architectural Engineering

August 2022

Graduate School of Engineering
Seoul National University
Architecture and Architectural Engineering
Seung Heon Lee

Confirming the Master's thesis written by
Seung Heon Lee

August 2022

Chair Sung-gul Hong (Seal)

Vice Chair Thomas Kang (Seal)

Examiner Hong-Gun Park (Seal)

Abstract

Parametric Study on the Design Methodology of Post-Tensioned Nuclear Containments with High Performance Concrete

Lee, Seung Heon
Department of Architecture and Architectural Engineering
College of Engineering
Seoul National University

Prestressed concrete containment vessels (PCCVs) play an important role in the safety of nuclear power plants, functioning as the final line of defense against the uncontrolled release of radioactive substances in the defense-in-depth safety philosophy of nuclear facilities. However, the construction of a concrete containment has historically been prone to many cost overruns and schedule delays overseas, which calls for qualitative leaps in PCCV design in order to maintain relevance and economic viability against competing steel containments.

The implementation of high performance concrete has the potential to reduce the amount of required reinforcing steel in a PCCV, which will reduce field labor as well as congestion. Concrete which exhibits high strength can allow for higher levels of prestressing, which can keep concrete in compression against postulated design accidents. In addition, cementitious materials reinforced with steel fiber such as ultra high-performance concrete (UHPC) are known to exhibit notable tensile ductility, and design guidelines which consider their tensile strength are being developed around the world.

However, there is a lack of codification effort with regard to utilizing high performance concrete in the design of concrete containments. This study performs parametric studies on the required volume of reinforcing steel according to parameters related to the implementation of high performance concrete. The variables are level of prestressing, the consideration of prestressing, concrete strength and the implementation of concrete tensile strength. Structural analysis is performed under primary factored loads defined in ASME BPVC III-2 using commercial finite element analysis software. Axial and flexural design is performed according to ASME Code Case N-850, while tangential shear design is performed according to ASME BPVC III-2. Also, the axial and flexural design methodology is expanded upon, where prestressing is considered as part of the axial/flexural capacity instead of a postulated load.

The results of the parametric study indicate that the consideration of prestressing as either demand or capacity affects the positional relationship between the P-M curves and factored loads, and consequently the resulting reinforcing steel layouts as well. The benefits of enhanced compressive strength mainly pertain to the increased maximum level of prestressing, and the direct alleviation in reinforcement requirements is marginal compared to the required strength increase. The consideration of tensile strength in UHPC, on the other hand, showed direct and meaningful reductions in reinforcing steel requirements.

While this study does not encompass all domains of design from conception to licensing, the results of this study are nonetheless expected to provide insights on the tendencies of reinforcing requirements according to enhanced mechanical properties of concrete, while adhering to design principles based on ASME Code.

Keywords: Concrete containment, high performance concrete, high strength concrete, UHPC, prestressed concrete, design code, ultimate strength design, P-M interaction curve, parametric study.

Student Number : 2020-27665

Contents

List of Tables

List of Figures

Chapter 1. Introduction

1.1 Motivation for research

Currently, amidst the high global interest in low carbon energy, nuclear power is still regarded as a valid energy source in transitioning from fossil fuels to renewable or low-carbon gases (European Commission, 2022). When nuclear power plants are in service, prestressed concrete containment vessels (PCCVs, **Figure 1-1**) function as a final line of defense against the uncontrolled release of radioactive substances in the defense-in-depth safety principle of nuclear facilities (Johnson et al., 2016). Concrete containments also provide effective radiation shielding and temperature resistance across nuclear plants' lifespans (Willam et al., 2013).

However, there have been historical cost overruns and schedule delays for PCCVs overseas, and advancements in the construction of concrete containments are required to maintain competitiveness against steel nuclear containments. Typically, to provide sufficient structural integrity under design loads as well as beyond design basis accidents, stringent code provisions and regulations with high levels of conservatism are in place for the design of concrete containments. This results in high amounts of steel reinforcements being required for the construction of PCCVs. While material costs themselves are not critical, this leads to less constructability and therefore increased labor costs, and also may relate to rebar congestion along with possible voids within the containment.

Studies indicate that the implementation of high performance materials can be one facet of improvement in lowering the levelized cost of electricity (LCOE) of nuclear facilities, including novel cementitious materials with higher compressive strength and enhanced tensile capacity (EPRI, 2018). Improvements in the mechanical performance of concrete and potentially

higher levels of prestressing may allow for the minimization or elimination of conventional rebar which would reduce both field labor as well as congestion.

However, there is a lack of sufficient theoretical and experimental research on establishing a design methodology for the implementation of such novel materials or relevant construction methods. This thesis seeks to study the how codified requirements for reinforcing steel may be alleviated with the use of novel cementitious materials, which exhibit higher compressive strength and drastically improved tensile ductility.

(a) Hanbit Nuclear Power Plant ("Hanbit Nuclear Power Plant," 2021)

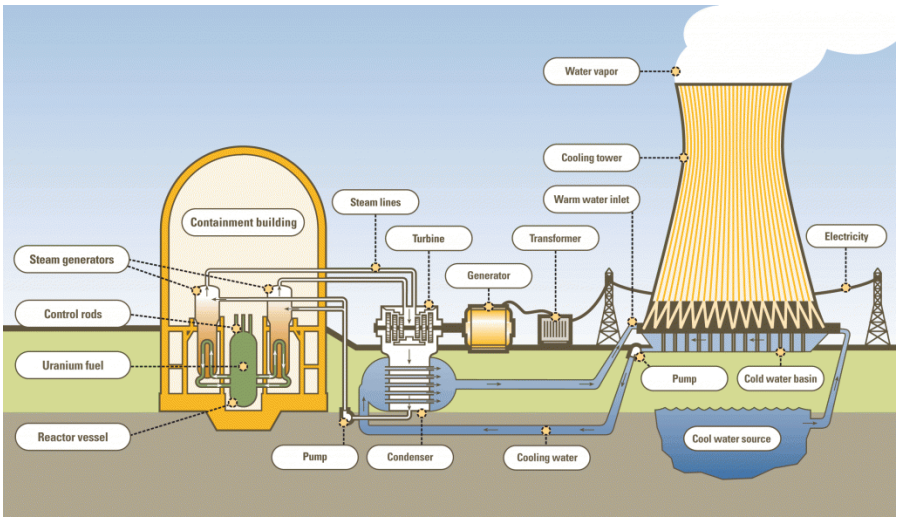

(b) Main features of nuclear power plants with PWR-type reactor ("Nuclear Power Plant | Definition, Principles & Components," n.d.)

Figure 1-1 Overview of PCCV in nuclear power plant

1.2 Scope and objective

Reinforcement design in this thesis refers to the combined application of ASME Code provisions for axial/flexural load design and those for tangential shear design, which govern the longitudinal reinforcement. The primary factored load criterion was taken for the analysis throughout this thesis. Parameters were chosen which have relevance to the mechanical properties of high performance concrete: maximum allowable level of prestressing, consideration of prestressing as either structural demand or capacity, concrete compressive strength and the consideration of concrete tensile strength.

The scope of this thesis relates strictly to the Design Basis Domain, where codified provisions govern the design. It can be said that the general scope of designing a PCCV from its initial conception to final licensing is truly vast, and the preliminary design is often modified according to various kinds of assessments supervised by regulatory organizations. However, the goal is not to provide a definitive conclusion for the implementation of high performance concrete in all aspects of containment design. Instead, this thesis aims to provide insights on its relation to the required reinforcing, which may act as the starting point for future codification efforts.

1.3 Organization

This thesis consists of six main chapters. **Chapter 1** introduces the motivation and scope of the research. **Chapter 2** is prefaced with the overall design domains and the role of post-tensioning in a PCCV. Thereafter, it details the reinforcement design methodology provided by ASME to be used throughout the thesis, as well as identifying areas of improvement from the implementation of high performance concrete. **Chapter 3** follows the structural analysis process which provides the design structural demands to be used in **Chapter 4** and **Chapter 5**. **Chapter 4** performs longitudinal reinforcement design for normal strength concrete, based on the ASME Code design methodologies outlined in **Chapter 2**. **Chapter 5** implements the constitutive laws of high performance concrete to the aforementioned design method, and also considers the contribution of concrete tensile capacity in the case of ultra high-performance concrete. **Chapter 6** presents the conclusions of this thesis.

Chapter 2. Review and Analysis of Design Methodologies and Codes

2.1 General design procedure of PCCVs

The design of PCCVs from their initial conception to standard reviews and licensing is largely divided into two subdomains: Design Basis and Design Extension (OECD NEA CSNI, 2015).

The Design Basis Domain deals with two categories typified as Design Basis Conditions such as loss of cooling accidents (LOCAs), and Design Basis Hazards such as seismic level 2 earthquakes (otherwise denoted as safety shutdown earthquakes, or SSEs) (IAEA, 2021; OECD NEA CSNI, 2015). The design principles for the Design Basis Domain are typically maintained by national codes and standards, some of which are shown in **Table 2-1**. In Korea, ASME Section III Division 2 (hereafter, ASME Code) or KEPIC SNB are used for the Design Basis Domain.

The Design Extension Domain deals with conditions and hazards more severe than those assumed in the design basis domain, referred to as beyond design-basis (BDB) accidents by the US Nuclear Regulatory Committee (US NRC). Design for this domain has more realistic assumptions which better secures the structural integrity of the PCCV structure. Deterministic and probabilistic evaluations are performed for events such as severe accidents and aircraft impacts (OECD NEA CSNI, 2015). The verification for this domain is typically not maintained by design codes, rather by regulatory organizations such as the US NRC and the Korean Institute of Nuclear Safety (KINS).

Table 2-1 List of standards and codes on PCCV design (OECD NEA CSNI, 2015)

Canada and internationally	• CSA N287.2-08, "Material Requirements for Concrete Containment Structures for CANDU Nuclear Power Plants", Canadian Standards Association, Mississauga, ON, 2008. • CSA N287.3-93, "Design Requirements for Concrete Containment Structures for CANDU Nuclear Power Plants", Canadian Standards Association, Rexdale, ON, 1993. • ASME III Division 2, "Code for Concrete Containments - Rules for Construction of Nuclear Facility Components", American Society of Mechanical Engineers", New York, NY, 2011. • ETC-C-2012, "EPR Technical Code for Civil Works", French Society for Design, Construction and In-Service Inspection Rules for Nuclear Island Components (afcen), Paris, 2012. • EJ/T 926-95, "The Design Code for the Prestressed Concrete Containment of the PWR NPP" Nuclear Industry Standards of the People's Republic of China.
Japan	• JSME S NE1-2011, "Rules on Concrete Containment Vessels for Nuclear Power Plants"
Russia	• NTD tema 08.05.50., “Standard on Design of Safety Important NPP Buildings”, Interatomenergo, Moscow 1989 • PiNAE G-10-007-89, “Standard on Design of Reinforced Concrete Structures of Safety Important NPP Buildings”, Gosatomenergonadzor USSR, Moscow 1989. • SNiP 2.03.01-84, “Concrete and Reinforced Concrete Structures)”, Gosstroy, Moscow 1985.
Sweden	• Kungliga Väg- och vattenbyggnadsstyrelsen, Statliga Betongbestämmelser 1949. (Oskarshamn 1) • Kungliga Väg- och vattenbyggnadsstyrelsen, Brobyggnadsanvisningar 1965. • Statens Planverks spännbetongnormer för husbyggnader SBN-S25:21, supplemented with AB Strängbetongs arbetsbeskrivning av den 10.4.1970.

It is typical to perform initial PCCV design in the Design Basis Domain, according to national codes and based on linear analyses. The preliminary design result is thereafter subjected to extensive evaluations in the Design Extension Domain, and this procedure is supervised by the national regulatory organization. If the containment design fails to provide an acceptable margin of safety, the design must be modified to observe the requirements (Moon et al., 2010). Only after sufficient safety reviews have been conducted and necessary changes have been made, can construction permits or operating licenses be issued (U.S. Nuclear Regulatory Commission, 2007a).

Currently, limited research has been performed on the effects that high performance concrete may have on the PCCV design procedure. Available literature mainly pertains to the effects of fiber reinforcement in the Design Extension Domain. The effects of fiber reinforcement on the ultimate pressure capacity of PCCVs was studied by Choun & Park (2015) and further investigated by Zheng et al. (2022), while its effects on aircraft impacts were examined by Seo & Noh (2013). Additionally, studies on effects towards the seismic shear capacity and impact resistance of PCCVs were conducted by Choun & Park (2015) and Jeon & Jin (2016), respectively.

On the other hand, in the Design Basis Domain, there is a lack of codification efforts which would consider the enhanced compressive strength or tensile ductility of novel cementitious materials. In order for PCCVs with high performance concrete to be accepted as an actual design option, it is desirable for advancements to be made in both domains of design. This thesis aims to provide reinforcing steel design methodologies and design examples based on the well-established ASME Code design philosophy, while also considering the effects of high performance concrete by implementing relevant standards which are accepted worldwide. This process is further specified in the following chapters.

2.2 Post-tensioning in PCCV design

2.2.1 Basic function and tendon layout

Internal pressure is one of the primary considerations for PCCV design, for both Design Basis and Design Extension Domains. ASME Code provides the load combination of Abnormal Loads, where design pressure P_a is multiplied by a load factor of 1.5, while a structural fragility assessment for overpressurization is requisite for severe accident evaluations (U.S. Nuclear Regulatory Commission, 2015). Such pressure loads exert membrane tensile stress on the containment structure, and significantly contributes toward PCCVs requiring a high volume of reinforcing steel.

Post-tensioning of concrete containments provides a direct method of resistance against inner pressure loads by limiting the resultant sectional forces and moments, as shown in **Figure 2-1**. As a result, wall thickness requirements compared to RC containments are alleviated by 300 ~ 600 mm (1 ~ 2 ft) (Moon et al., 2010). The concrete being kept under compression also minimizes crack formation, keeping the containment as leaktight as possible in the absence of steel liners or complementary coating, as well as improving the reversibility of the structural response (OECD NEA CSNI, 2015). Considering the role of containment structures as a final barrier, it can be said that the post-tensioning system is the cornerstone of maintaining the structural integrity of a PCCV.

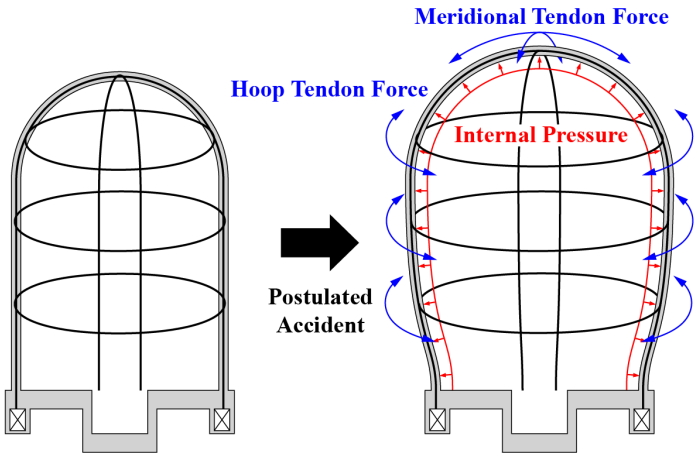

Figure 2-1 Role of post-tensioning in PCCVs

A concrete containment typically consists of a cylindrical wall with a dome placed on top to function as a pressure vessel. Prestressing tendons are inserted in a set configuration of ducts within a containment shell, and post-tensioned at both ends. **Figure 2-2(a)** exemplifies some of the tendon layouts adopted around the globe, which differ in directionality and anchorage locations. For this thesis, a pre-existing PCCV design with a hemispherical dome is assumed, which has a tendon layout consisting of hoop and meridional tendons (**Figure 2-2(b)**). The characteristics of this layout provide the basis upon which they will be idealized and the prestressing forces be modified for the parametric study.

Hoop tendons are placed along the horizontal direction of the containment up to the 45º point at the dome, each spanning two-thirds of the circumference and anchored at two of three buttresses. Each tendon is shifted by 120º along the containment height to obtain a globally uniform distribution of tendon forces. Hoop tendons are placed closer to the outer surface to minimize radial tensile stress (Choi, 2018), located at around three-quarters of the wall thickness. This is because hoop tendons in the cylindrical wall exhibit the greatest tendon forces per unit area. For analysis purposes in the Design Basis Domain, hoop tendons are assumed to span along the entire circumference, and instead spaced 1.5 times the actual spacing (**Figure 2-2(c)**).

Meridional tendons are placed along the vertical direction of the containment in an inverted U-shape. These tendons do not exert inward force at the cylindrical wall due to a lack of curvature, only acting inward at the dome. Despite the axisymmetric geometry of the overall containment, meridional tendons are configured in one of two perpendicular directions as shown in **Figure 2-2(b)**. Meridional tendons in the two directions act together near the dome apex above the 45º point, while tendons in one direction and the dome hoop tendons act together below this point. Unlike hoop tendons, meridional tendons are located around the midpoint of the wall thickness, but slightly offset at the dome to provide sufficient spacing between the tendons in two directions. This minimizes any eccentricities at the containment wall which may cause unwanted sectional moment loads.

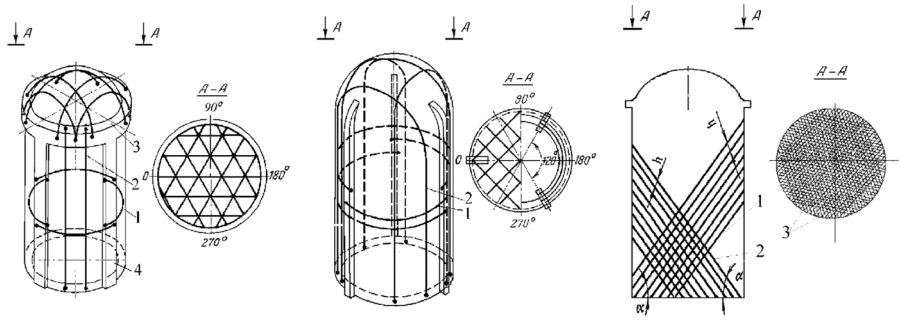

(a) PCCV tendon layout schemes (Freidin & Krichevsky, 2002)

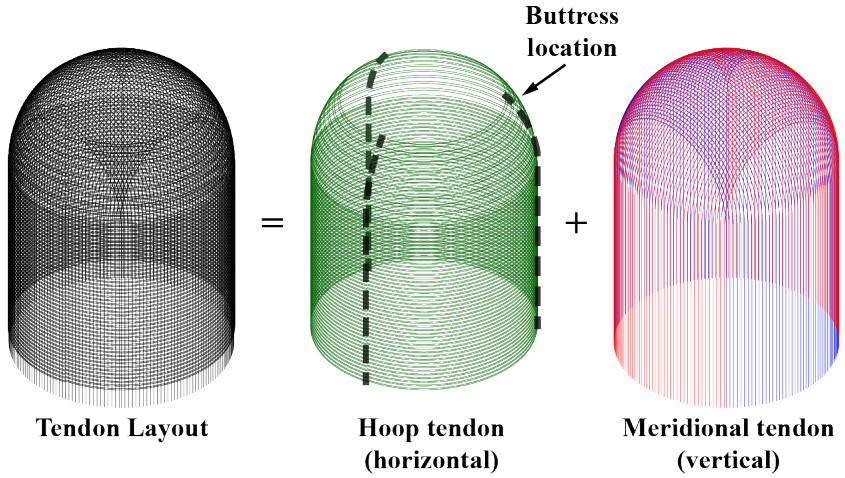

(b) Assumed tendon layout for thesis

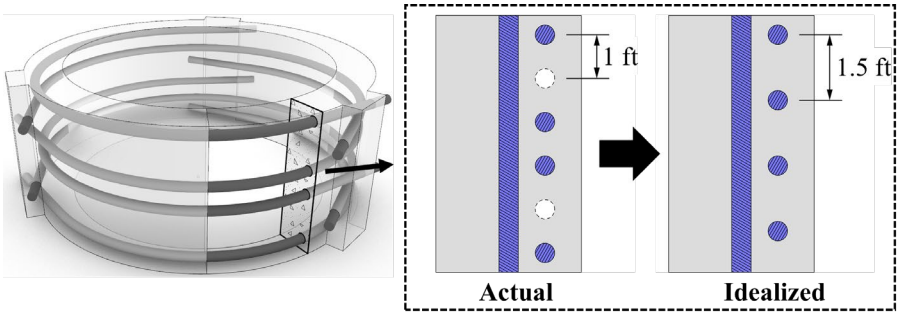

(c) Hoop tendon layout and idealization (Conversion: 1ft = 305 mm)

Figure 2-2 PCCV tendon layout

2.2.2 Concept of level of prestressing

As previously mentioned, the prestressing of concrete containments directly offsets internal pressure loads. In the Design Basis Domain, the required prestressing force as well as the corresponding amount of prestressing steel are commonly determined according to how much inner pressure is balanced out relative to the design pressure load. For example, the first generation of PCCVs in the United States had effective prestress designated to be 1.5 times design accident pressure P_a, and PCCVs currently in service are typically designed for a value between $1.0 \sim 1.5P_a$.

This leads into the term 'level of prestressing' used in PCCV design, denoted as X in ASME Code Commentary and defined as **Eq. (2-1)**. X can be determined for a particular tendon layout approximated as inward forces which would then be expressed in terms of its ratio to the postulated design pressure. This conversion is performed via **Eq. (2-2)**, also taken from the Code Commentary. The q obtained from **Eq. (2-2)** corresponds to the inward force for a unit tendon length of 1 ft or 305 mm (**Figure 2-3(a)**), which are then converted to an equivalent inward surface pressure by dividing q by the effective tendon spacing.

$$X = \frac{Q}{P_a} \qquad \textbf{(2-1)}$$

where: X = Level of prestressing

Q = Balancing load from prestressing

P_a = Design pressure load

$$q = \frac{F}{R} \qquad \textbf{(2-2)}$$

where: q = Normal force exerted by tendon per unit length

F = Tendon force

R = Radius from center point

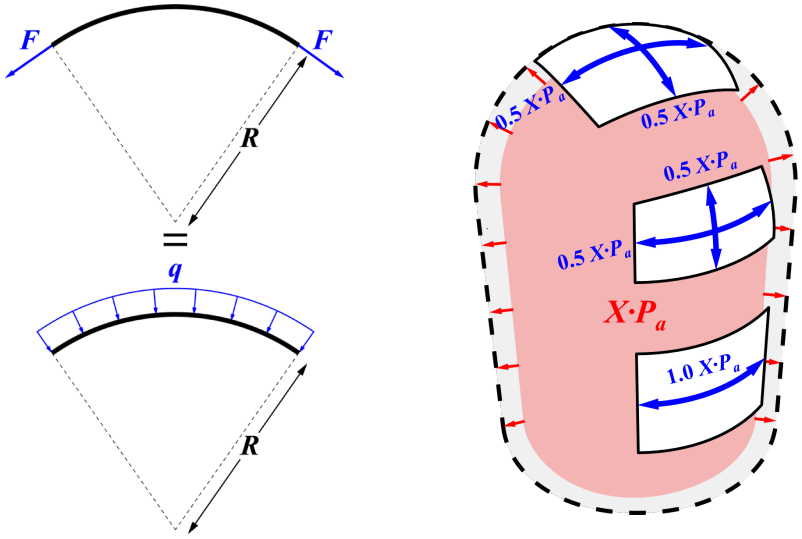

(a) Conversion of tendon force to inward load

(b) Distribution of balancing loads for single and double curvature

Figure 2-3 Conversion and load balancing of prestressing

The tendons in one direction are not necessarily designed to account for the full $X{\cdot}P_a$, as depicted in **Figure 2-3(b)**. It is only at the cylindrical wall with single curvature that the hoop tendons must balance out 1.0 $X{\cdot}P_a$. At the dome which has double curvature, a pair of either the hoop and meridional tendons or the meridional tendons in perpendicular directions are assumed to account for 0.5 $X{\cdot}P_a$ each, depending on the location at the dome (Johnson et al., 2016).

In essence, the concept of level of prestressing is an extension of the load balancing principle for conventional prestressed concrete design. Nonetheless, this denotation is quite useful in in the design of concrete containments, because of how it provides insight on the core design principle of PCCVs with regards to internal pressure and prestressing. The denotation of X will be used throughout this thesis, as the primary variable for the parametric study.

2.2.3 Maximum level of prestressing

To close off this subchapter, the relation between concrete strength and the maximum allowable level of prestressing is investigated. While the post-tensioning is indeed integral for a PCCV to maintain structural integrity, it is important to note that the maximum tendon force per unit area is limited by an allowable limit of $0.3f_c'$ by ASME Code. The maximum level of prestressing, denoted X_{max} for this thesis, can be determined by obtaining the hoop tendon force at the cylindrical wall corresponding to an average compressive stress of $0.3f_c'$, and deriving the consequent level of prestressing X.

An example is given for a unit volume of an axisymmetric cylindrical shell, with inner radius R, wall thickness t, tendon force F, where the tendon is located at a distance t' and the inner surface set as 1' × 1' (or 305 mm × 305 mm) (**Figure 2-4(a)**). X_{max} is obtained such that the outward force F_{inner} and inward force F_{outer} are equal, where F_{outer} is derived from the tendon force F corresponding to ASME allowable limits. **Eq. (2-3)** ~ **Eq. (2-5)** can be rearranged to obtain **Eq. (2-6)**, and the parameters are shown on a sectional diagram in **Figure 2-4(b)**. Note that 1 means 1 ft. or 305 mm.

From **Eq. (2-6)** it can be seen that when the design pressure, inner shell radius and wall thickness are given, X_{max} can be expressed as a linear function of concrete strength, leading to the topic of study in thesis regarding high performance concrete. This equation will be used in **Chapter 2.5** to obtain maximum levels of prestressing for a multitude of concrete classes as defined in European standards.

$$F = 0.3f_c' \cdot 1 \cdot t = 0.3f_c't \tag{2-3}$$

$$F_{inner} = XP_a \cdot 1 \cdot 1 = XP_a \tag{2-4}$$

$$F_{outer} = \left(\frac{F}{R+t'}\right) \cdot \left(\frac{R+t'}{R}\right) = \frac{F}{R} \tag{2-5}$$

$$X_{\max} = \frac{0.3f_c't}{P_aR} \tag{2-6}$$

where: F_{inner} = Inward force exerted by tendon

F_{outer} = Outward force exerted by inner pressure

$X_{\max}$ = Maximum level of prestressing

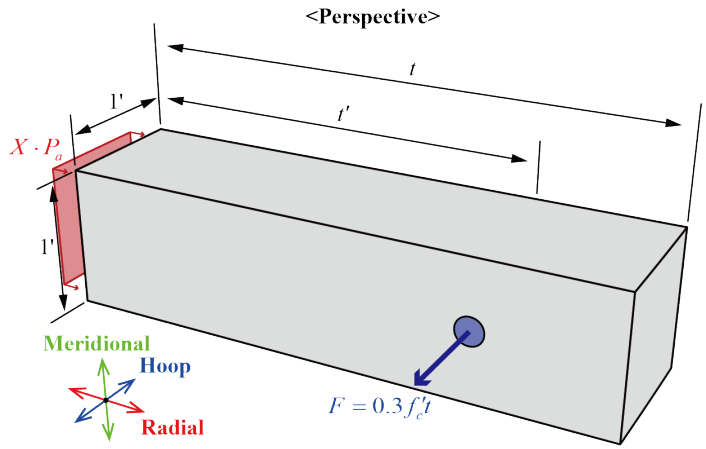

(a) Perspective diagram

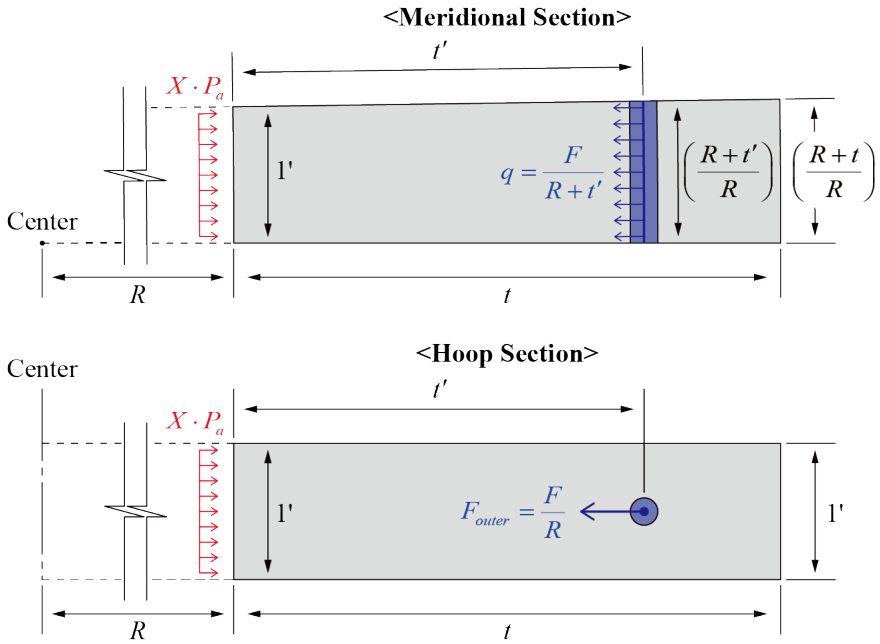

(b) Sectional properties and parameters

Figure 2-4 Assumed unit volume for X_{max} derivation (Conversion: 1' = 305 mm)

2.3 ASME provisions for axial and flexural design

2.3.1 Introduction and basic assumptions

For longitudinal reinforcement design, ASME Code provides allowable stress and strain values as the main design consideration, commonly referred to as the Allowable Stress Design (ASD) method, as opposed to the strength design method adopted in ACI 349 and ACI 318, whose Strength Design (SD) method only defines sectional capacities and corresponding strength reduction factors (Johnson et al., 2016). This design philosophy is taken in order to keep the entirety of the containment essentially elastic under service loads and within postulated limits under factored loads. This allows for more direct control over concrete cracks and helps maintain a certain degree of leak tightness under design accident conditions (Bae, 2011). **Table 2-2** and **Table 2-3** specify the given allowable stress or strain limits for concrete and reinforcing steel.

The allowable limits are subdivided along two categories: 1) membrane stress versus membrane plus bending stress, and 2) primary force versus primary plus secondary forces. Membrane stress is defined as the average of normal stress along the wall thickness, while bending stress is defined as its variable component (Joint ACI-ASME Committee, 2019). It goes to follow that integrating membrane stresses results in axial force while integrating bending stress times distance from the centroid results in flexural moments.

Table 2-2 Summary of allowable stress of concrete in ASME (Bae, 2011)

		Membrane plus bending	Membrane
Factored loads	(1) Primary	$0.75f_c'$	$0.60f_c'$
	(2) Primary plus secondary	$0.85f_c'$ *	$0.75f_c'$
Service loads	(3) Primary	$0.45f_c'$	$0.30f_c'$ ($0.35f_c'$ **)
	(4) Primary plus secondary	$0.60f_c'$	$0.45f_c'$

* Maximum allowable stress of $0.85f_c'$ corresponds to limiting strain of 0.002.

** At initial prestress.

Table 2-3 Summary of allowable limits of rebar in ASME (Bae, 2011)

		Membrane plus bending	
		Stress	Strain
Factored loads	(1) Primary	$0.90f_y$	ε_s may exceed $0.9\varepsilon_y$ but not exceed $2\varepsilon_y$
	(2) Primary plus secondary	$0.90f_y$	ε_s may exceed $0.9\varepsilon_y$
Service loads	(3) Primary	$0.50f_y$ ($0.67f_y$ *)	$0.50\varepsilon_y$ ($0.67\varepsilon_y$ *)
	(4) Primary plus secondary	$0.67f_y$	$0.67\varepsilon_y$

* During prestressing.

Primary forces are defined as the reactionary internal forces or moments required to equilibrate applied design loads. On the other hand, secondary forces do not directly equilibrate applied loads, mainly referring to forces and moments resulting from volume change effects such as shrinkage strain or thermal strain. Such secondary loads exert stress only under conditions of restraint, and may be self-relieving due to mechanisms such as cracking, yielding, relaxation or creep (ACI Committee 349, 2014). Because of this, when secondary forces are considered in tandem with primary forces, concrete is allowed to reach up to the assumed peak stress of $0.85f_c'$ while the strain limits for reinforcement are alleviated for service loads and lifted for factored loads (Johnson et al., 2016).

The uniaxial constitutive laws assumed for design purposes are depicted in **Figure 2-5**. For factored loads, the compressive stress-strain relationship of concrete is assumed to be parabolic, where post-peak behavior is not allowed due to the brittle nature of concrete. For service loads, ASME Code specifies use of a linear constitutive relationship, where the compressive strain is multiplied by the modulus of elasticity E_c. Similar to ACI 318, the tensile strength of concrete is ignored in the design process. The stress-strain relationship of the reinforcing steel is assumed to be elasto-perfectly plastic.

The parabolic compressive law for concrete is multiplied by a factor of 0.85 for factored loads while the stress at reinforcing steel is bound by f_y multiplied by a factor of 0.9. The factors of 0.85 and 0.9 essentially act as strength reduction factors from the SD philosophy, only that they are applied separately to the

concrete and steel, which is similar in practice to the partial safety factors for Eurocode. The ASME Code allowable limits, in tandem with the modified constitutive laws, provides the necessary conservatism in lieu of strength reduction factors utilized in ACI 349 and ACI 318.

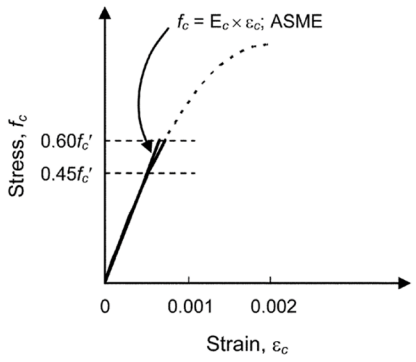

(a) Stress-strain curve of concrete under service loads

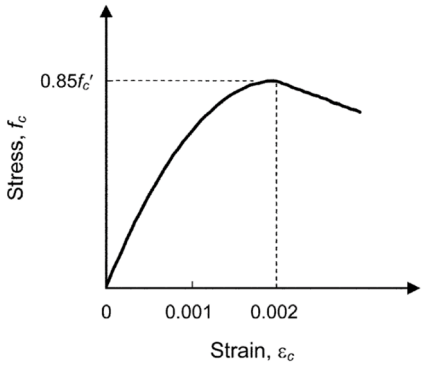

(b) Stress-strain curve of concrete under factored loads

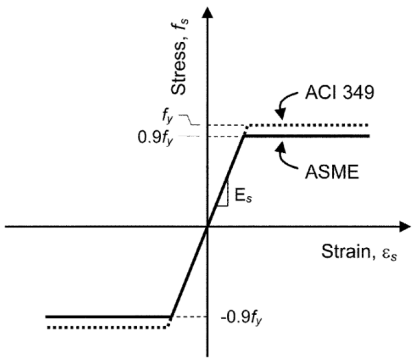

(c) Stress-strain curve of reinforcing steel

Figure 2-5 Uniaxial constitutive law for ASME Code (Bae, 2011)

2.3.2 Axial and flexural load design methodology

This subchapter describes a reinforcement design methodology for axial and flexural loads utilizing P-M interaction curves, and also introduces a further streamlined method akin to the Strength Design philosophy, proposed by Bae (2011) and accepted as ASME Code Case N-850. This method will provide the basis for axial and flexural design throughout this thesis, and expanded upon for the constitutive laws of high performance concrete.

In principle, the stress and strain at all locations along the containment sections must be checked for compliance with the aforementioned allowable limits, for both membrane and membrane plus bending categories. It is also acceptable to utilize P-M interaction curves constructed according to ASME Code allowable limits, and thereafter compare them to the axial force and flexural moments integrated from sectional stresses (Bae, 2011), which is similar to the SD philosophy in that sectional capacities are assumed with the allowable limits as bases.

Such an approach of utilizing P-M curves provides visual representations of the structural capacity and demands, but require complex calculations due to the nonlinear stress-strain relationship of concrete. Due to this complication, it is typical to reduce computational loads by discretizing the concrete cross sections as a series of rectangular layers, where strain is assumed to be uniform at each layer and the corresponding uniform stresses at the layers are obtained from assumed constitutive laws and integrated to obtain the sectional axial force and moments. This procedure is named the layer-by-layer analysis technique, or fiber analysis technique. By repeating this process for multiple strain distributions whose maximum values are bound by allowable limits for membrane plus bending stress, P-M curves can be constructed for primary and primary plus secondary forces, under service loads and factored loads. **Figure 2-6(b)** shows an example of P-M interaction curves obtained from this process, for the sectional and material assumptions laid out in **Figure 2-6(a)**. The allowable limits for membrane stress and corresponding axial forces act as the upper bound for the P-M curve, which results in the cutoff on the compression side for the curves.

ASME Code Case N-850 provides a further streamlined method of constructing a P-M curve, which is taken from Bae (2011). This method utilizes the equivalent rectangular concrete stress block, first pioneered by Whitney (1937) and adopted in the SD methodology of ACI 349 and ACI 318. The basic concept of this alternate method is to provide modified factors to the stress block defined for the SD method such that the acceptance criteria and constitutive laws provided in ASME Code would be satisfied. Three parameters are introduced: 1) α_1, defining the average concrete stress relative to specified compressive strength, 2) β_1, defining the depth of the equivalent stress block relative to the distance from extreme compression fiber to neutral axis, and 3) $\varepsilon_{c,allow}$, defining the allowable concrete strains corresponding to the defined allowable stresses. The proposed values for each load criteria are shown in **Table 2-4**.

The parameter $\varepsilon_{c,allow}$ is derived from the assumed constitutive laws for factored and service loads with their corresponding allowable limits, acting as the postulated strain at the extreme compression fiber. The two parameters α_1 and β_1 are computed such that the stress block provides equivalent average concrete stress and centroid compared to the stress distribution from the neutral axis to the extreme compression fiber, as depicted in **Figure 2-7(a)**.

The values of α_1 and β_1 according to the postulated allowable stress are depicted in **Figure 2-7(c)**, and the exact values at the four load criteria are shown in **Table 2-5**. It is interesting to note that the values of α_1 calculated from allowable limits for membrane plus bending stress agree reasonably well with the allowable limits for membrane stress in **Table 2-2**, with the exception of α_1 = 0.3375 for primary forces under service loads, at no prestress conditions. Because of this, the proposed α_1 values in **Table 2-4** are taken from the allowable membrane stress limits, while the calculated α_1 value is taken for service primary load conditions, where an upper limit of axial strength corresponding to concrete stress of $0.3f_c'$ is placed if no prestress is applied. β_1, on the other hand, is presented as a uniform value of 0.70 due to its small range of fluctuation.

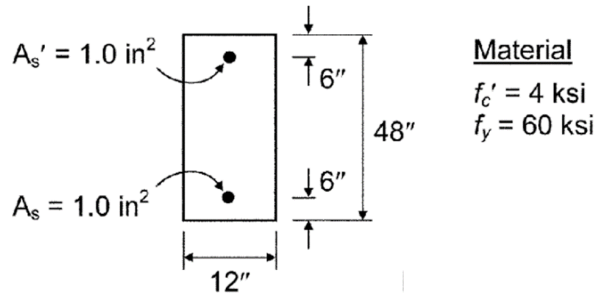

(a) Assumed section and material properties for example P-M curve
(Conversion: 1in. = 25.4 mm; 1 ksi = 7 MPa)

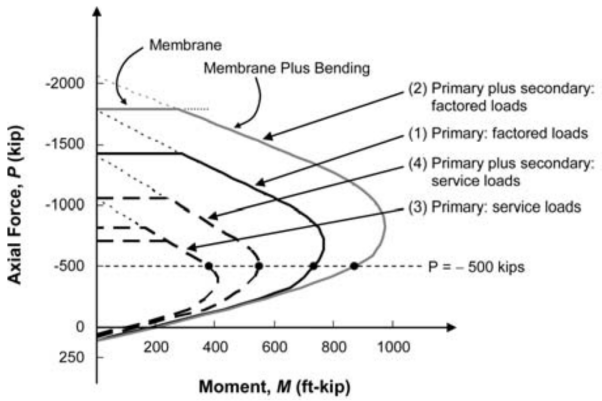

(b) P-M curves according to design load criteria
(Conversion: 1 kip = 4.45 kN; 1 ft-kip = 1.356 kN-m)

Figure 2-6 P-M curve construction according to ASME Code (Bae, 2011)

Table 2-4 Concrete stress block parameters for alternate USD method (Bae, 2011)

		α_1	β_1	$\varepsilon_{c,allow}$
Factored loads	Primary	0.60	0.70	0.0013
	Primary plus secondary	0.75	0.70	0.0020
Service loads	Primary*	0.34	0.70	$0.45f_c'/E_c$
	Primary plus secondary	0.45	0.70	$0.60f_c'/E_c$

*At no prestress conditions, compressive axial strength shall be limited to
$P_{allow} = 0.30f_c'A_c + (0.30f_c'E_s/E_c)A_s$

Table 2-5 Exact values of α_1 and β_1 calculated for equivalent stress block

		α_1	β_1
Factored loads	Primary	0.6114	0.7134
	Primary plus secondary	0.7556	0.7500
Service loads	Primary*	0.3375	0.6667
	Primary plus secondary	0.4500	0.6667

One additional consideration for constructing P-M interaction curves is for strain distributions after the tensile strain of the reinforcement reaches the allowable limit, as depicted in the central strain distribution of **Figure 2-6(a)**. Because ASME Code provides allowable strains for reinforcing steel as opposed to ACI 349, where a limit is not specified, ultimate strength with regards to reinforcing steel can be defined where the concrete compressive strain is below $\varepsilon_{c,allow}$. In this case, Bae (2011) proposes that the stress block be scaled down by the ratio of compressive strain at the extreme fiber to $\varepsilon_{c,allow}$, as shown in **Figure 2-7(b)**.

Using the three parameters of α_1, β_1 and $\varepsilon_{c,allow}$ derived from ASME Code provisions and obtaining sectional capacities with the concrete stress block, P-M interaction curves can be constructed with a process analogous to the conventional SD methodology. **Figure 2-7(d)** depicts the P-M interaction curves constructed from this method for the concrete section of **Figure 2-6(b)**, together with the P-M curves derived directly from the allowable limits. The curves obtained from the Code Case N-850 agree well with the design strengths obtained from the ASME design philosophy.

The curves tend to provide more conservative predictions for factored loads, whereas they slightly overestimate the structural capacity for service loads. However, it should be noted that ASME Code assumes a linear stress-strain relationship for concrete under service loads, as depicted in **Figure 2-5(a)**. This idealization tends to underestimate design strength compared to a nonlinear parabolic relation, which is depicted as dashed lines in **Figure 2-7(d)**. Therefore, it can be said that the ultimate strength method nevertheless provides sufficient estimations for the ASME Code load criteria, with a more simplified approach that conforms to conventional RC design methodology.

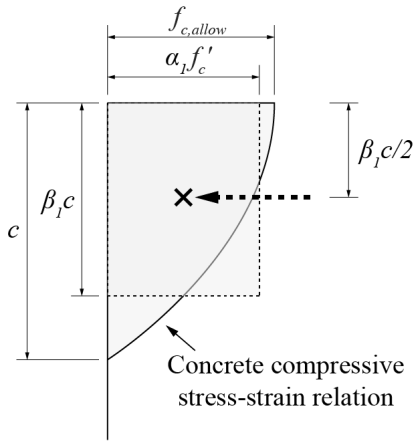

(a) Definition of concrete rectangular stress block for ASME

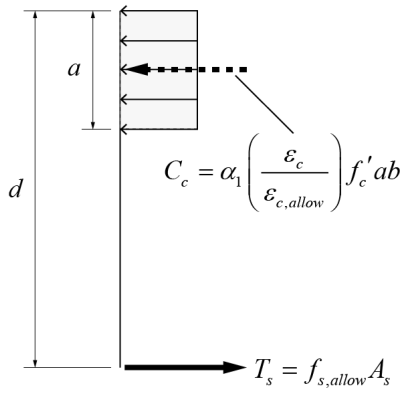

(b) Modified stress block at steel allowable tensile strain

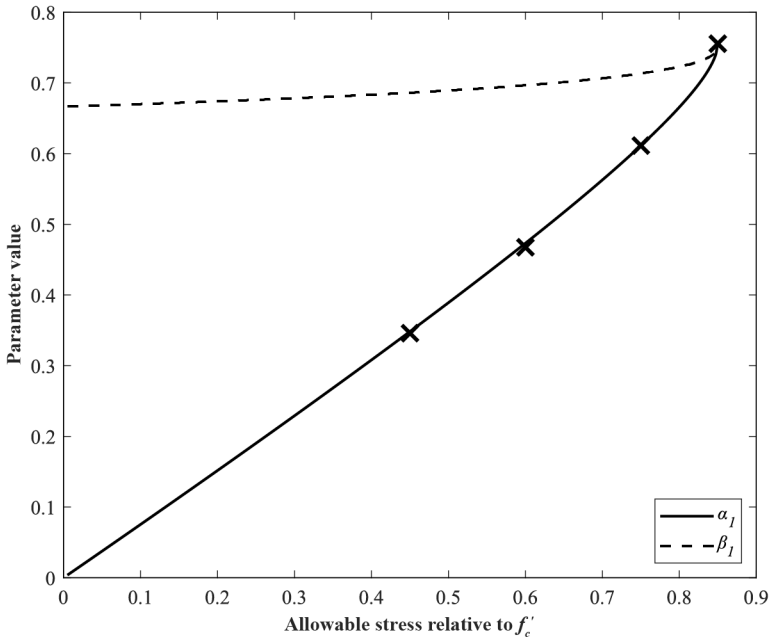

(c) Parameter values according to allowable stress limit

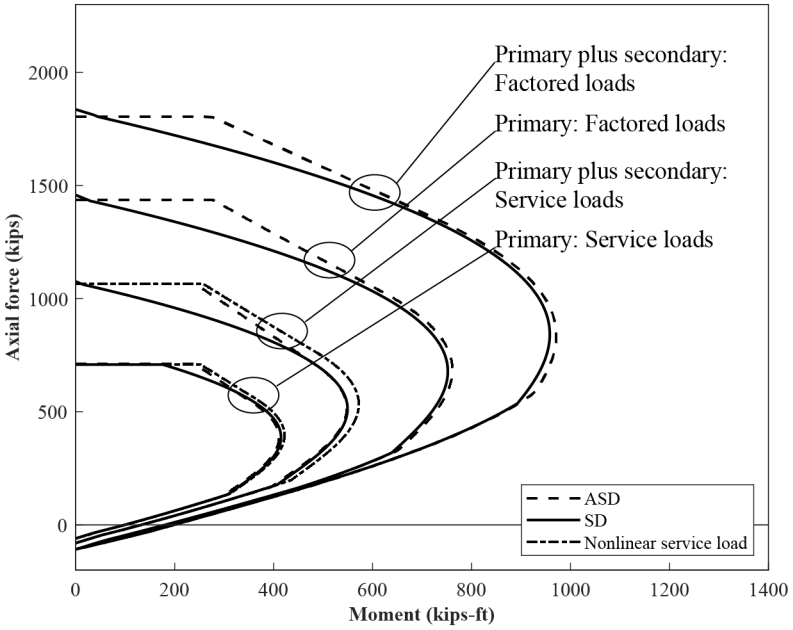

(d) Comparison of P-M interaction curves constructed from
ASME Code and Code Case N-850
(Conversion: 1 kip = 4.45 kN; 1 kips-ft = 1.356 kN-m)

Figure 2-7 Derivation of Code Case N-850 and comparison with ASME Code
(redrawn from Bae, 2011)

2.3.3 Consideration of prestressing in sectional capacity

This section provides an additional step in the axial and flexural design of PCCVs, in considering prestressing steel as part of the sectional capacities represented by P-M interaction curves. An example is presented where a P-M curve is generated under the primary factored load criteria specified in the previous chapter. In this procedure, a reinforced concrete (RC) section with prestressing steel is considered for obtaining the axial and flexural capacity.

Typically, it is an accepted method of PCCV analysis to take the effects of prestressing as a structural demand, and convert them to equivalent prestressing forces. In this case, the design loads and resultant structural responses are preemptively balanced out by the prestressing force, after which conventional RC design is performed. Such an approach is considered appropriate for elastic analyses which are utilized in the Design Basis Domain (Abrishami et al., 2015). However, it is the contention of this thesis that implementing prestressing steel as part of the structural capacity would better account for some characteristics of prestressing, primarily regarding the hoop tendons.

As aforementioned, hoop tendons at the cylindrical wall (hereafter referred to as the 'shell' for brevity) are placed closer to the outer surface, and exhibit the largest tendon forces for the PCCV design assumed in this thesis. In other words, prestressing force is highest where there exists a notable tendon eccentricity. When prestressing is considered as part of design loads, hoop tendon forces are input as equivalent loads and are the structural responses are derived via linear analysis. In this case, the effects of prestressing would result in membrane compressive stress, and the effects of such eccentricity would be lost in obtaining the sectional capacity. In order to obtain a more accurate relation between postulated demand and sectional capacity at ultimate, the axial and flexural strength should be derived considering the combined interactions of concrete, reinforcing steel and prestressing steel. **Figure 2-8** depicts the two methods of considering prestressing loads covered in this thesis.

Research on P-M interaction curve generation for prestressed concrete sections has primarily been performed for symmetric sections on the compressive side (Kim, 2011; Naaman, 2004; Salmons & McLaughlin, 1982; Valaparambil et al., 2014), such as the P-M curves in **Figure 2-9**. However, PCCVs are different

from concrete columns in that hoop tendons are placed with eccentricity, and membrane tensile stresses due to LOCAs are a primary design concern. The asymmetric section requires construction of P-M curves for both positive and negative moment capacity, while the tensile loads require curves to be extended to the negative side of axial capacity.

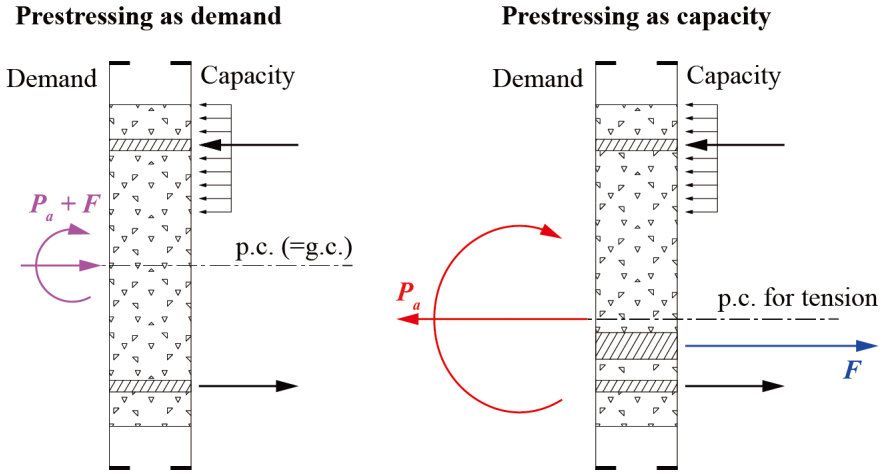

Figure 2-8 Methods of prestressing consideration

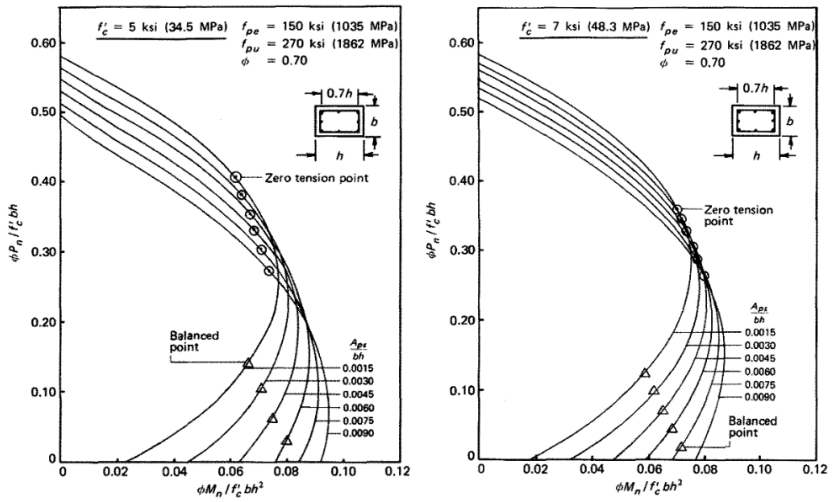

Figure 2-9 Non-dimensional load-moment interaction diagrams for prestressed concrete square and rectangular columns (Naaman, 2004)

An important thing to note for would be obtaining the plastic centroid (p.c.), around which the moments are calculated (Christou et al., 2011). By definition, plastic centroids are defined as the centroid of an RC section in its 'plastic' state, i.e., all reinforcing steel has yielded and concrete has reached maximum compressive strength across the entire section (Fafitis, 2001; Wang & Salmon, 1998). When generating P-M interaction curves, this corresponds to a state of uniform maximum compressive strain, which sets the moment capacity to zero at maximum axial load capacity (Christou et al., 2011).

If an RC section has a symmetric rebar layout, the p.c. would coincide with the geometric centroid (g.c.). However, for asymmetric sections, the location of the p.c. must first be obtained to generate the P-M curve, and data points corresponding to the axial and flexural loads must also be reconfigured around the p.c. The PCCV shell in the hoop direction is inherently asymmetric regardless of the reinforcing steel due to the tendon eccentricity, and thus the p.c. is a prominent point of interest. Also, unlike concrete columns, PCCVs are subject to membrane tensile stresses under design pressure, and moments paired with tensile axial forces should be obtained around a plastic centroid for a 'tensile plastic state.' As tensile strength of concrete is ignored in axial and flexural design for ASME Code as well as ACI 318, this corresponds to a case of uniform tensile strain across the section, and reinforcing steel has yielded in tension. At this state, the prestressing steel exerts a considerable amount of tensile force, and the p.c. is shifted towards the outer surface even if the rebar layout is symmetric.

ASME Code provides reinforcing steel strain limits for all load cases except factored primary plus secondary load criteria (**Table 2-3**), so the specific value of tensile strain can be defined in the case of PCCV design. As for the prestressing steel, the stress corresponding to this uniform tensile strain distribution would be determined depending on whether the PCCV is bonded or unbonded. Bonded PCCVs inject cementitious grout into the ducts after post-tensioning, and the prestressing steel can be assumed to follow the concrete sectional strain. In this case, the sectional strain can be directly translated to the strain variation $\Delta\varepsilon_{ps}$, and the corresponding stress f_{ps} can be obtained through **Eq. (2-7)**. The value of f_{ps} is bound by an upper limit of $0.9f_{py}$ as per ASME Code, similar to the constitutive law for reinforcing steel (**Figure 2-5(c)**).

$$f_{ps} = f_{se} + \Delta f_{ps} = f_{se} + E_p \Delta \varepsilon_{ps} \leq 0.9 f_{py} \quad \textbf{(2-7)}$$

where: f_{ps} = Stress in unbonded prestressing steel at nominal strength

f_{se} = Effective prestress in unbonded tendons after losses

Δf_{ps} = Stress increase in unbonded tendons beyond effective prestress

E_p = Modulus of elasticity of prestressing steel

$\Delta \varepsilon_{ps}$ = Strain increase in prestressing steel beyond effective prestress at critical section

Unbonded PCCVs, commonly used in Korea and the United States, present a challenge in obtaining an exact solution for f_{ps}. Unlike their bonded counterparts, the stress at unbonded tendons is member-dependent instead of section-dependent (Yang & Kang, 2011); that is to say, changes in strain across an unbonded tendon are normalized, and the exact tendon strain at the critical section cannot be obtained without information at the member-level. While there is no singular consensus on code equations for f_{ps}, studies indicate that performing a compatibility analysis with a strain reduction coefficient Ω_u, ranging from 0.0 ~ 1.0, is a reasonable approach with good accuracy (Alqam et al., 2021; Yang & Kang, 2011). For example, Yang & Kang (2011) provide **Eq. (2-8)** in obtaining f_{ps}, where Ω_u is determined according to prestressing reinforcement ratio, span-depth ratio, and tendon profile.

$$f_{ps} = f_{se} + \Delta f_{ps} = f_{se} + E_p \Omega_u \left(\frac{d_p - c}{c} \right) \varepsilon_{cu} \quad \textbf{(2-8)}$$

where: Ω_u = strain reduction coefficient at ultimate

d_p = depth from extreme compression fiber to centroid of prestressing steel

c = depth of neutral axis at ultimate

ε_{cu} = strain of concrete extreme compression fiber at ultimate

It is questionable, however, whether methods of obtaining Δf_{ps} for unbonded post-tensioned beams could be considered as equally valid for PCCVs. Beams typically have a clearly defined critical section at midspan, where it is checked

for nominal flexural capacity. The sectional strain distributions across their spans can also be clearly defined according to the loading method and boundary conditions.

Concrete containments, on the other hand, are composed of a cylindrical wall and a dome, where postulated design accidents induce biaxial tensile axial force and/or bending moments. Such complexity makes it difficult to pinpoint a single critical section for which to obtain a strain reduction coefficient. Even in the hoop direction, where the load combinations with axisymmetric input loads govern, it would be unrealistic to assume sectional strain compatibility of tendons ($\Omega_u = 1$), because that would essentially assume that the ultimate state occurs concurrently at all sections throughout this direction. There is also a lack of experimental data on the member-level structural response of an entire PCCV under postulated design loads, which would be required to verify the validity of any strain reduction coefficients derived analytically. Because of the limitations of PCCV design mentioned above, this thesis opts to assume that the stress at prestressing steel remains as f_{se} (**Eq. (2-9)**) regardless of the sectional strain distribution, i.e., $\Omega_u = 0$.

$$f_{ps} = f_{se} \tag{2-9}$$

P-M interaction curves are generated with the assumptions of **Figure 2-10(a)**, for Ω_u = 0.0, 0.35, 0.7 and 1.0. **Figure 2-10(b)** depicts the curves in the meridional direction (d_p = 24 in. or 610 mm), and **Figure 2-10(c)** depicts curves in the hoop direction (d_p = 36 in. or 914 mm). Both figures show the bonded assumption resulting in the largest sectional capacity, whereas the P-M curves constructed with $\Omega_u = 0$ for this thesis are the most conservative.

The red lines show the eccentricity of membrane tensile stress around the p.c, which are typically the governing loads for axial and flexural design in the hoop direction. By definition, membrane tensile stresses would act uniformly across the containment section at the g.c., and exert zero moment for symmetric sections such as in the assumed meridional direction. On the other hand, for the hoop direction, the p.c. is shifted towards the outer surface, and the eccentricity membrane tensile stresses are shifted towards the left side, in the negative moment direction.

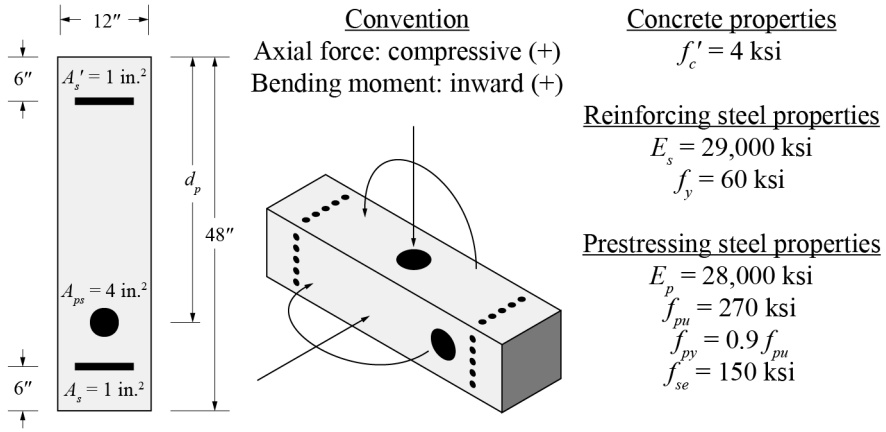

(a) Assumed sectional properties for P-M curve
(Conversion: 1 in. = 25.4 mm; 1 ksi = 7 MPa)

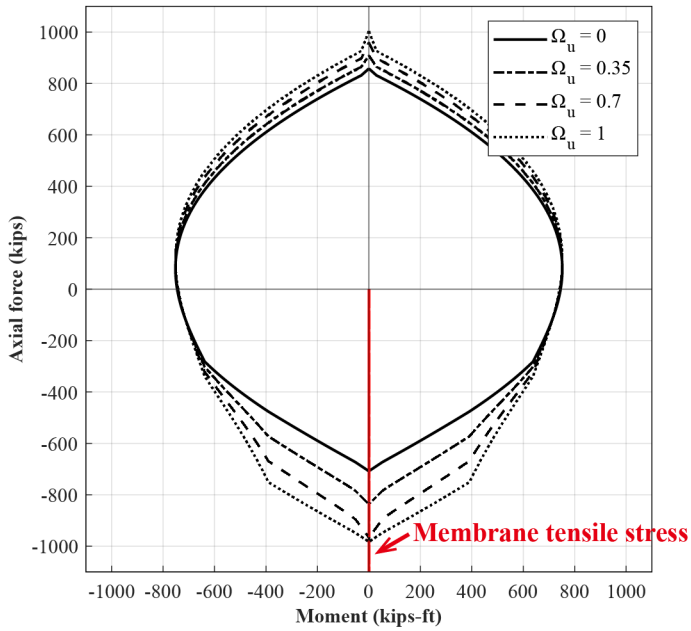

(b) P-M curves for d_p = 24 in. or 610 mm (meridional section)
(Conversion: 1kip = 4.45 kN; 1 kips-ft = 1.356 kN-m)

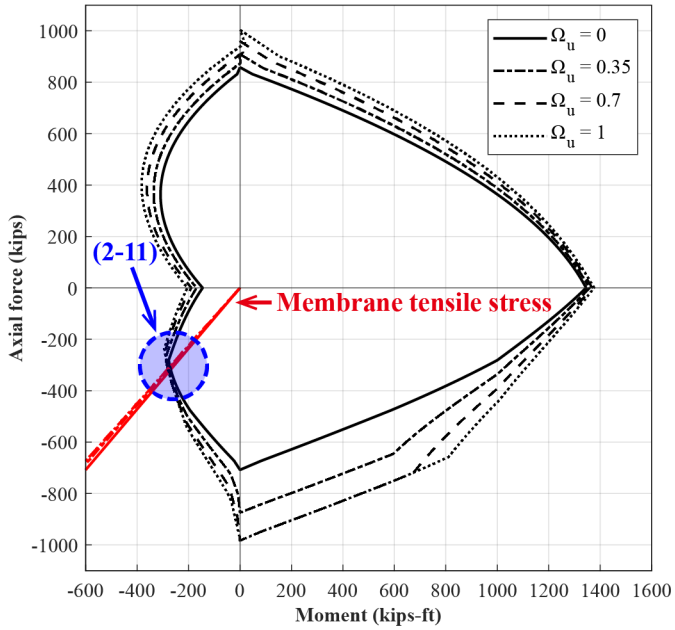

(c) P-M curves for d_p = 36 in. or 914 mm (hoop section)
(Conversion: 1kip = 4.45 kN; 1 kips-ft = 1.356 kN-m)

Figure 2-10 P-M interaction curves for prestressing as sectional capacity

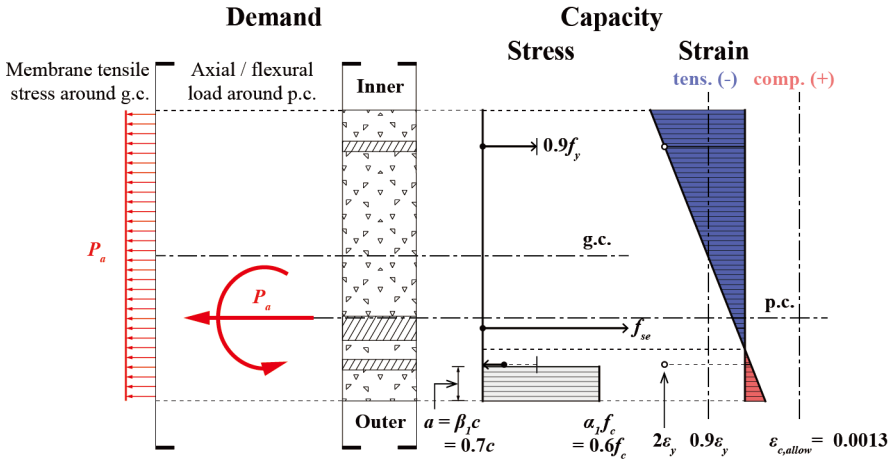

Figure 2-11 Sectional capacity at ultimate against membrane tensile stress

The structural capacity and demand for hoop sections coincide at the third quadrant, as depicted in the blue circle of **Figure 2-10(c)**. **Figure 2-11** shows the force equilibrium for membrane tensile stress and its corresponding ultimate state. Because there is a shift in the p.c., the tensile load is resisted in part by the concrete compressive strength in tandem with the reinforcing and prestressing steel. This suggests that for hoop sections with notable tendon eccentricity, concrete strength would affect the axial and flexural load capacity against membrane tensile loads.

To further investigate the relationship between prestressing steel and concrete strength, P-M curves in the hoop section are drawn for prestressing steel areas A_{ps} = 0 in.^{2}, 2 in.^{2}, 4 in.^{2} and 6 in.^{2} (0 mm^2, 1290 mm^2, 2580 mm^2 and 3870 mm^2) as shown in **Figure 2-12(a)**. It can be seen that increasing the A_{ps}, and consequently the prestressing force, shifts the P-M interaction curve towards the bottom right (tension, positive moment) side. On the other hand, the eccentricities of membrane tensile stresses are shifted to the left as A_{ps} increases, as previously shown in **Figure 2-10(c)**.

These shifts in separate directions for the P-M curves and governing loads result in a peculiarity in the capacity-demand relationship. In **Figure 2-12(a)**, increasing the prestressing steel area results in capacity improvements up to A_{ps} = 4 in.^{2} (2580 mm^2), being able to withstand larger magnitudes of membrane tensile stress. However, as A_{ps} is increased to 6 in.^{2} (3870 mm^2), the P-M curve configuration is shifted to the point that it geometrically cannot encompass any loads in the line of membrane tensile stress eccentricity. In this case, reinforcing steel requirements would be increased in order to enlarge the P-M curve towards the left side.

This phenomenon occurs because the force equilibrium of **Figure 2-11** results from combined actions of the concrete stress block and the prestressing force. As the prestressing force is increased via A_{ps}, there will be a threshold where the concrete strength is insufficient to constitute this force equilibrium. It goes to follow that increasing the compressive strength would counteract this occurrence.

In **Figure 2-12(b)**, f_c' is increased from 4 ksi to 7 ksi (28 MPa to 49 MPa) for A_{ps} = 6 in.^{2} (3870 mm^2). It can be seen that the P-M curve is enlarged towards

the top side, resulting in an increase in capacity against the governing loads. However, the efficacy of incremental strength increase is lessened for higher values of f_c', due to concrete strength mainly acting as a means to offset the increased prestressing force. Once f_c' is increased such that the P-M interaction curve can encompass loads along the line of eccentricity, the capacity increase against membrane tensile loads is minimal.

To conclude, this section expanded upon the SD methodology proposed by Bae (2011), where the prestressing is considered part of the sectional capacity. This method provides P-M curves which would better reflect the sectional stress and strain conditions at ultimate, due to the shift in plastic centroid in the hoop direction. The relationship between membrane tensile stress and corresponding ultimate state was investigated, as well as its interactions with prestressing steel area and concrete strength. In later chapters, reinforcement design will be performed such that the requirements from considering prestressing as both capacity and demand are satisfied, as to provide sufficient conservatism.

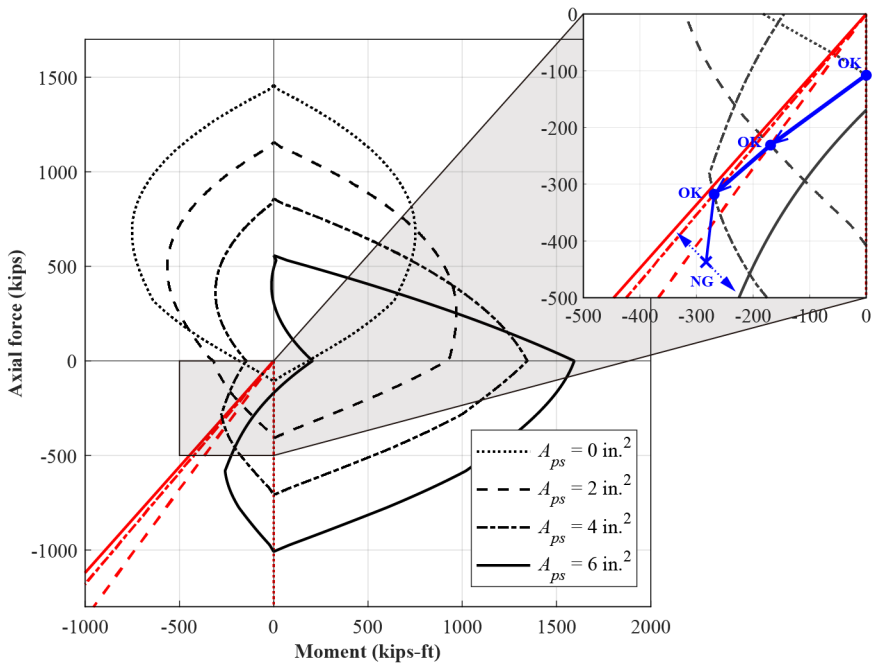

(a) P-M curves for hoop section and f_c' = 4 ksi (28 MPa) according to A_{ps}
(Conversion: 1 kip = 4.45 kN; 1 ksi = 7 MPa; 1 kips-ft = 1.356 kN-m)

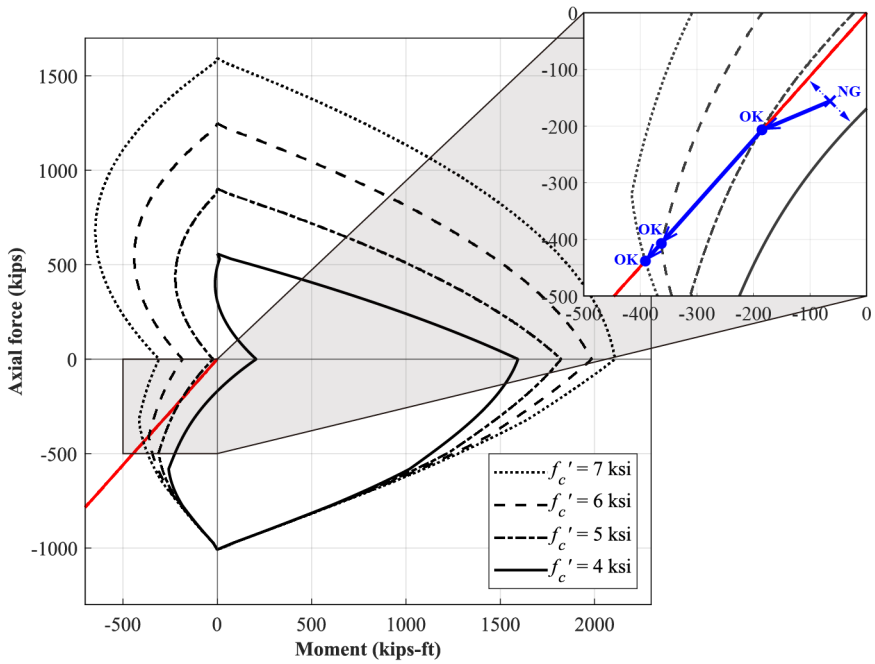

(a) P-M curves for hoop section and A_{ps} = 6 in.^{2} (3870 mm^2) according to f_c'
(Conversion: 1 kip = 4.45 kN; 1 ksi = 7 MPa; 1 kips-ft = 1.356 kN-m)

Figure 2-12 Parametric study of P-M interaction curves according to prestressing steel area and concrete strength

2.4 ASME provisions for tangential shear design

This subchapter provides background information on ASME Code provisions for tangential shear, which are the in-plane shear forces along the containment wall typically governed by seismic loads, and also relate to the design of longitudinal reinforcement in PCCVs. Background information on the derivation of relevant equations can be found in Appendix E of ASME Code Commentary (Johnson et al., 2016).

The previous chapter introduced items for axial and flexural loads where allowable stress and strain limits were the main design considerations, along with elements of Strength Design in reduction factors for constitutive laws. Provisions for tangential shear, on the other hand, are closer in design philosophy to SD in the sense that there are no allowable stress or strain criteria, rather the design is performed such that the sectional capacity obtained from concrete or steel meet the structural demands from postulated tangential shear loads. Also, whereas axial and flexural load provisions relate to both service and factored loads, tangential shear provisions are only given for factored loads because they are governed by the design accidents.

However, a significant difference exists between the ASME Code approach to tangential shear and that of ACI 349 and ACI 318, in the consideration of concrete shear strength after initial cracking. ACI 318-19 provisions provides nominal shear strength equations which consider the contribution of both the reinforcement and concrete after crack initiation. This can be seen in ACI provisions such as **Eq. (2-10)** for one-way shear, **Eq. (2-11)** for two-way shear, and for in-plane shear of RC walls, **Eq. (2-12)**.

$$V_n = V_c + V_s \tag{2-10}$$

$$v_n = v_c + v_s \tag{2-11}$$

$$V_n = \left(\alpha_c \lambda \sqrt{f'_c} + \rho_t f_{yt}\right) A_{cv} \tag{2-12}$$

where: V_n = nominal shear strength, lbf (N)

V_c = nominal shear strength provided by concrete, lbf (N)

V_s = nominal shear strength provided by shear reinforcement, lbf (N)

v_n = equivalent concrete stress corresponding to nominal two-way shear strength of slab or footing, psi (MPa)

v_c = equivalent concrete stress corresponding to nominal shear strength provided by concrete, psi (MPa)

v_s = equivalent concrete stress corresponding to nominal two-way shear strength provided by reinforcement, psi (MPa)

α_c = coefficient defining the relative contribution of concrete strength to nominal wall shear strength

λ = modification factor for lightweight concrete

f'_c = specified compressive strength of concrete, psi (MPa)

ρ_t = ratio of area of distributed transverse reinforcement to gross concrete area perpendicular to that reinforcement

f_{yt} = specified yield strength of transverse reinforcement, psi (MPa)

A_{cv} = gross area of concrete section bounded by web thickness and length of section in the direction of shear force considered in the case of walls, in.^{2} (mm^2)

Conversely, ASME Code does not assume a scenario where concrete and reinforcement contribute concurrently to resist tangential shear loads, and two design cases are considered where either the concrete or the reinforcing steel bears the full tangential shear force. Such a dichotomic approach was taken because PCCVs in the Design Basis Domain are designed to resist a combination of biaxial tension and tangential shear, due to LOCAs and seismic loads such as OBEs and SSEs, respectively.

At the time of provision establishment, there was insufficient experimental evidence to presume that concrete shows a meaningful capacity to transfer shear strength under a state of biaxial tension, and it was conservatively assumed that concrete contribution would be taken as zero under cracked assumptions (Johnson et al., 2016). In the case where sufficient prestressing is provided such that the containment remains in net compression under design loads the tangential shear strength of concrete would be taken, but the

contribution of the reinforcing steel would be ignored because the load bearing capacity of reinforcement only initiates after concrete cracking.

ASME provisions specify requirements for the design case where concrete strength is considered, where: 1) a containment is prestressed, 2) concrete is kept in net compression for both hoop and meridional directions, 3) effects of thermal membrane forces i.e. secondary effects are included in forces, and 4) the concrete tangential shear strength, denoted V_c, satisfies **Eq. (2-13)**. The value of V_c in **Eq. (2-14)** is obtained from a Mohr's circle with elastic assumptions owing to the net compression, where a principal tensile strength of $4\sqrt{f_c'}$ (U.S. units) or $\frac{\sqrt{f_c'}}{3}$ (SI units) is taken from ACI 318. V_c is multiplied by a strength reduction factor of 0.85 to be compared with the given tangential shear force V_u. Because the load bearing capacity of reinforcing steel initiates only after concrete has cracked, no additional considerations for reinforcing are required.

$$V_c \le 0.85 V_c \qquad \textbf{(2-13)}$$

$$V_c = 4\sqrt{f_c'}bt\sqrt{1+\left[\frac{f_m+f_h}{4\sqrt{f_c'}}\right]+\left[\frac{f_m f_h}{\left(4\sqrt{f_c'}\right)^2}\right]} \text{ (U.S. units)}$$

$$V_c = \frac{\sqrt{f_c'}}{3}bt\sqrt{1+\left[\frac{f_m+f_h}{\frac{\sqrt{f_c'}}{3}}\right]+\left[\frac{f_m f_h}{\left(\frac{\sqrt{f_c'}}{3}\right)^2}\right]} \text{ (SI units)} \qquad \textbf{(2-14)}$$

where: V_c = tangential shear strength provided by concrete

f_h and f_m = membrane stresses respectively in meridional and hoop directions, compression positive, psi (MPa)

b = assumed section width for calculation, in. (mm)

t = wall thickness, in. (mm)

When the above conditions are not met, the reinforcing steel area in the hoop and meridional direction must be designed so that they provide sufficient

tangential shear strength, as shown in **Eq. (2-15)** and **Eq. (2-16)**. These equations are derived from calculating force equilibrium from the free body diagram shown in **Figure 2-11**. The square root of sum of squares is taken for the biaxial and shear forces due to seismic loads, separate from the other design loads, to obtain their combined representative value. The yield stress of the reinforcement is multiplied by a strength reduction factor of 0.9.

Additional limits to the tangential shear strength provided by orthogonal reinforcement, V_{so}, and the tangential shear force, V_u, are given in **Eq. (2-17)** and **Eq. (2-18)**, respectively. These limits are given to prevent diagonal crushing failure and sliding shear failure in shear transfer mechanisms (Johnson et al., 2016). In the case of a 2-way layout without inclined reinforcement, **Eq. (2-17)** and **Eq. (2-18)** result in **Eq. (2-19)**, which is higher than the limit for nominal in-plane shear strength of walls in ACI 318, at $V_n \le 8\sqrt{f'_c}A_{cv}$ (U.S. units) or $V_n \le 0.66\sqrt{f'_c}A_{cv}$ (SI units).

Overall, the items for tangential shear act as companion provisions to those for axial and flexural loads in determining the required reinforcement area throughout the containment sections. If the requirements for considering concrete tangential shear capacity are met, then the provisions for axial and flexural loads would govern; otherwise, design for both criteria must be performed and the more conservative result should be taken.

$$A_{sh} + A_{si} \ge \frac{N_h + \left(N_{hl}^2 + V_u^2\right)^{\frac{1}{2}}}{0.9 f_y} \qquad \textbf{(2-15)}$$

$$A_{sm} + A_{si} \ge \frac{N_m + \left(N_{ml}^2 + V_u^2\right)^{\frac{1}{2}}}{0.9 f_y} \qquad \textbf{(2-16)}$$

$$V_{so} = V_u - 0.9 f_y A_{si}$$

$$V_{so} \le 10\sqrt{f'_c}bt \quad \text{(U.S. units)} \qquad \textbf{(2-17)}$$

$$V_{so} \le 0.83\sqrt{f'_c}bt \quad \text{(SI units)}$$

$$V_u \le 20\sqrt{f_c'}bt - V_{so} \quad \text{(U.S. units)}$$
$$V_u \le 1.66\sqrt{f_c'}bt - V_{so} \quad \text{(SI units)} \qquad \textbf{(2-18)}$$

$$V_u \le 10\sqrt{f_c'}bt \quad \text{(U.S. units)}$$
$$V_u \le 0.83\sqrt{f_c'}bt \quad \text{(SI units)} \qquad \textbf{(2-19)}$$

where: A_{sh} = area of bonded reinforcement in the hoop direction, in.^{2}/ft (mm^2/m)

A_{si} = area of bonded reinforcement in one direction of inclined bars at 45 deg to horizontal, in.^{2}/ft (mm^2/m) along a line perpendicular to the direction of the bars. Inclined reinforcement shall be provided in both directions.

A_{sm} = area of bonded reinforcement in the meridional direction, in.^{2}/ft (mm^2/m)

N_h and N_m = membrane force in the hoop and meridional direction respectively due to pressure, prestress, and dead load, lbf (N). The prestress force shall be the effective value. N_h and N_m are positive when tension and negative when compression.

N_{hl} and N_{ml} = membrane force in the hoop and meridional direction, respectively, from lateral load such as earthquake, wind, or tornado loading, lbf (N). When considering earthquake loading, this force is based on the square root of the sum of the squares of the components of the two horizontal and vertical earthquakes. The force is always considered as positive.

V_u = the peak membrane tangential shear force resulting from lateral load such as earthquake, wind, or tornado loading, lbf (N). When considering earthquake loading, this force is based on the square root of the sum of the squares of the components of the two horizontal and vertical earthquakes. The shear force shall be considered as positive.

V_{so} = tangential shear strength provided by orthogonal reinforcement, lbf (N)

V_{si} = tangential shear strength provided by inclined reinforcement, lbf (N)

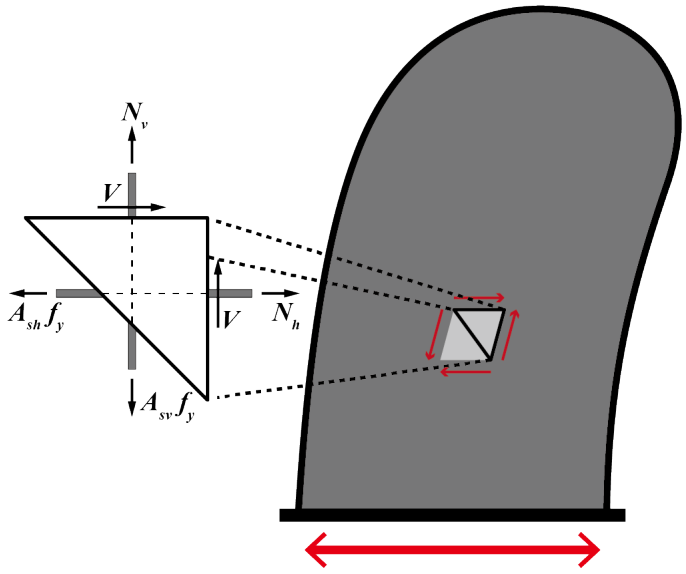

Figure 2-13 Free body diagram for diagonal tension equilibrium*
(Redrawn from Johnson et al., 2016)

*meridional direction described as vertical direction

2.5 Considerations for high performance concrete

This subchapter investigates areas to expand upon the reinforcement design methodologies stated in the previous chapters, taking into account the properties of high performance concrete.

Before discussing the possible improvements, it should first be noted that current American codes do not provide a consistent design guideline which is maintained by a single committee. ACI 318 provides guidance valid for normal strength concrete of $f_c^{'}$ < 8,000 psi (55 MPa), whereas high strength concrete and UHPC are covered in ACI 363R and ACI 239R, respectively, both of which are maintained by separate committees and function as reports rather than as definitive design codes. In the case of ASME Code, there are no provisions which consider the usage of high strength concrete or UHPC.

Because of this, the Eurocode classification of concrete is used in defining the concrete classes and properties throughout this thesis, because it provides consistent constitutive laws for characteristic cylinder compressive strengths up to 90 MPa (13,050 ksi). For UHPC, the French standard NF P18-710 provides indicative values to be used for preliminary analyses, as well as design laws for both compression and tension. NF P18-710 is also presented as an addition to Eurocode 2, providing analogous provisions in consideration of the properties of UHPC. This thesis performs longitudinal reinforcement design using material properties of concrete classes C30/37 through C90/105 taken from Eurocode 2, and properties of UHPC taken from NF P18-710. An initial analysis is performed for C30/37 to examine the design procedure in detail, after which the process is performed for the other concrete classes as a parametric study.

In implementing concrete with enhanced mechanical properties, the first improvement that can be expected is the increase in allowable level of prestressing according to concrete compressive strength. As X_{max} increases, more portions of the factored design pressure will be balanced out, possibly extending to pressure loads postulated in the Design Extension Domain. It was mentioned in **Section 2.2.3** with **Eq. (2-6)** that X_{max} can be expressed as a linear function of concrete strength. For the containment configuration and design

parameters to be assumed in **Chapter 3.1**, where t = 4 ft (1.2 m), R = 72 ft (21.9 m) and P_a = 54 psi (0.37 MPa), **Eq. (3-1)** can be obtained.

$$X_{\max} = \frac{f_c'}{3,240} \quad \text{(US unit)}$$
$$X_{\max} = \frac{f_c'}{22.34} \quad \text{(SI unit)} \qquad \textbf{(2-20)}$$

Table 2-6 shows the values of X_{max} for some concrete classes to be considered in this thesis, where the specified concrete compressive strength f_c' defined in American codes is replaced with the characteristic concrete compressive strength f_{ck} defined in Eurocode. Improvements in compressive strength further than C90/105 are not expected to be meaningful for PCCV design, as the ultimate pressure capacity of concrete containments is observed to be between 3.0P_a and 4.0P_a (Sandia National Laboratories, 2003).

Table 2-6 Maximum level of prestressing according to allowable membrane stress

Concrete class	f_{ck}*	X_{max}
C30/37	4,350 psi (30 MPa)	1.34
C60/75	8,700 psi (60 MPa)	2.69
C90/105	13,050 psi (90 MPa)	4.03
UHPC	25,400 psi (175 MPa)	7.84

*Taken in place of specified concrete compressive strength

The second area of potential improvement brought by the implementation of high performance concrete pertains to the method of constructing P-M curves in the hoop direction with prestressing considered as capacity (**Section 2.3.3**). It was observed that the particular ultimate state corresponding to the line of eccentricity of membrane tensile stress is attained from the collective actions of concrete, reinforcing steel and prestressing steel. As hoop tendons exhibit the greatest tendon forces with notable eccentricity, enhanced compressive capabilities are expected to result in improvement in reinforcing requirements, especially at higher levels of prestressing where sufficient concrete strength is required to constitute the force equilibrium.

The third, and perhaps the most promising area of improvement, is in considering the contribution of the concrete tensile strength in the design process. Design codes around the world such as ACI 318, Eurocode and ASME Code disregard the tensile strength of concrete in axial and flexural design, due to the brittle behavior of concrete. However, fiber-reinforced cementitious materials such as UHPC are being developed worldwide and exhibit notable and tensile ductility compared to conventional concrete. The implementation of such tensile properties into sectional design can potentially alleviate reinforcing steel requirements to a significant degree, especially because biaxial tension due to internal pressure is a primary consideration for both the Design Basis and Design Extension Domains.

In response to the enhanced mechanical properties of UHPC, flexural design methodologies have been developed around the world (AFNOR, 2016; CSA, 2019; SIA, 2016). Although the United States has yet to see a formal design guideline for UHPC, research is underway to develop guidelines which agree with previous ACI Conventions (El-Helou & Graybeal, 2019, 2022). As previously mentioned, the French guideline NF P18-710 provides a framework of design for UHPC structural components (ACI Committee 239, 2018), which is consistent with Eurocode 2 provisions. The methodology of NF P18-710 is used as the baseline for implementing UHPC tensile strength in PCCV design.

A parametric study of reinforcement design according to the concrete class is performed in **Chapter 5**, in light of the observations made in this section. The compressive stress-strain relationships are redefined according to Eurocode 2 and NF P18-710, and rectangular stress block parameters which were given in **Table 2-2** are recalculated accordingly. The tensile stress-strain relationship defined according to NF P18-710 is simplified into a tensile stress block which yields a closed P-M curve which is sufficiently conservative compared to the exact solution. The results of the analysis will provide insight into the effects of implementing high performance concrete on the longitudinal reinforcement design of PCCVs.

Chapter 3. Structural Analysis of Containment

3.1 Analysis assumptions

3.1.1 Assumed parameters for design loads

Structural analysis and parametric studies of longitudinal reinforcement design are performed for the factored primary load criteria herein. The structural response of a PCCV design with concrete class C30/37 from Eurocode 2 is obtained through finite element analysis (FEA) via the software DIANA. The resulting sectional forces derived from this analysis serve as data points which would be compared with P-M curves derived from the SD procedure outlined in the previous chapter.

For the containment modeling, a PCCV design with a hemispherical dome and orthogonal tendon layout is assumed, as depicted in **Figure 3-1(a)** and **(b)**. The containment is modeled as axisymmetric and 3D FEA models depicted in **Figure 3-1(c)** and **(d)**, where analysis is performed with linear elastic assumptions as per ASME Code. Mesh sizes are set at 2′ for the meridional and hoop directions, and 0.5′ for the through-thickness direction. **Table 3-1** shows the material properties of the concrete taken from Eurocode 2.

Design loads are taken from subsection CC-3200 of ASME Code, where gravity loads (dead load, D and live load, L), prestressing loads (F), design pressure loads (P_a) and seismic loads (operating basis earthquake, E_o and safe shutdown earthquake, E_{ss}) are considered. The postulated load combinations are shown in **Table 3-2**.

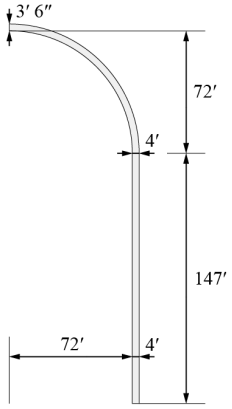

(a) Containment configuration

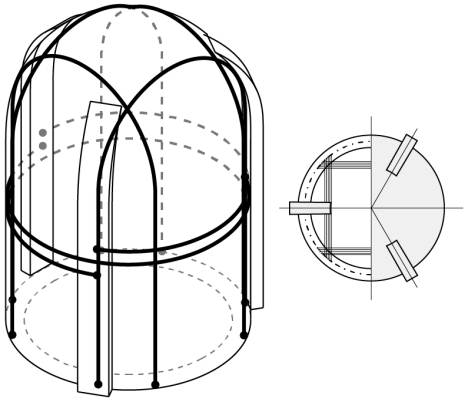

(b) Tendon layout diagram
(Redrawn from Freidin & Krichevsky, 2002)

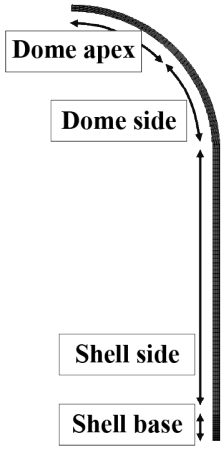

(c) Axisymmetric FEA model

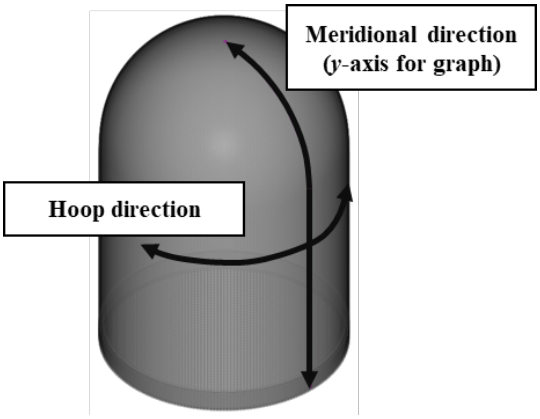

(d) 3D FEA model

Figure 3-1 Assumed PCCV design for structural analysis

Table 3-1 Material properties of concrete class C30/37 for structural analysis

Category	Value
Characteristic cylinder compressive strength f_{ck}	4,350 psi * (30 MPa)
Mean cylinder compressive strength f_{cm}	5,500 psi * (38 MPa)
Modulus of elasticity E_{cm}	4,750 ksi * (33 GPa)
Poisson's ratio	0.2
Density w_c	156 pcf (2500 kg/m^3)

* Rounded to the nearest multiple of 50

The specific values used for the FEA are shown in **Table 3-3**. The dead load is taken from the assumed concrete density in **Table 3-1**, while the live load, design pressure load and peak ground acceleration (PGA) are taken from typical parameters for in-service nuclear containments. When prestressing is considered as demand, it is input indirectly by converting prestressing forces corresponding to $X = 1$ into equivalent surface loads.

Thereafter, linear static analysis is performed for the axisymmetric model where the gravity loads, equivalent prestressing loads and design pressure loads are considered. Structural responses to seismic loads are considered implicitly through response spectrum analysis (RSA) for the 3D model. Because concrete is assumed to be elastic in this analysis, the structural response to each design load can be obtained separately and superposed for each load combination.

Table 3-2 Considered load combinations for primary loads (ASME Code)

Category		Load factors
Factored loads	Abnormal	$1.0D + 1.0L + 1.0F + 1.5P_a$
	Abnormal/severe environmental	$1.0D + 1.0L + 1.0F + 1.25P_a + 1.25\ E_o$
	Abnormal/extreme environmental	$1.0D + 1.0L + 1.0F + 1.0P_a + 1.0\ E_{ss}$

Table 3-3 Design load parameters

Design load		Input values
Dead load (D)		156 pcf (2500 kg/m^3)
Live load (L)		50 psf (244 kg/m^2)
Design Pressure (P_a)		54 psi (0.37 MPa)
Prestressing load* (F)	Vertical tendons	270 kips/ft (3,940 kN/m)
	Wall hoop tendons	560 kips/ft (8,173 kN/m)
	Dome hoop tendons	270 kips/ft (3,940 kN/m)
Operating basis earthquake (E_o)	PGA	0.1g (horizontal) 0.065g (vertical)
	Modal damping ratio	0.03
Safe Shutdown Earthquake (E_{ss})	PGA	0.2g (horizontal) 0.13g (vertical)
	Modal damping ratio	0.05

* Values taken for $X = 1.0$

3.1.2 Considerations for seismic load

Response spectrum analysis is performed following regulatory guides (RGs) provided by the US Nuclear Regulatory Committee (USNRC), to obtain the representative maximum response due to E_o or E_{ss}. As per RG 1.92, the responses for three orthogonal ground motions (two horizontal and one vertical) are obtained via Complete Quadratic Combination (CQC), as shown in **Eq. (3-1)**. In obtaining the modal correlation coefficient ε_{ij}, RG 1.92 allows calculation methods presented by Rosenblueth or Der Kiureghian, and this study utilizes the Der Kiureghian coefficient native to DIANA (**Eq. (3-2)**). The peak ground accelerations for SSE are set as 0.2g for horizontal and 0.13g for vertical, while those for OBE are set as half the SSE values. The damping ratios for SSE and OBE are set as 5% and 3%, respectively, as per RG 1.60. The corresponding design response spectra are determined from RG 1.61, which are depicted in **Figure 3-2**.

Modal combination is performed up to the 100th mode, and the complete representative seismic response of the containment is obtained by combining responses for the three directions via Square Root of the Sum of the Squares (SRSS) method.

$$R_{pl} = \left[\sum_{i=1}^{n} \sum_{j=1}^{n} \varepsilon_{ij} R_{p_i} R_{p_j} \right]^{\frac{1}{2}} \quad \textbf{(3-1)}$$

where:

R_{pl} = combined periodic response for the I^{th} component of seismic input motion (I = 1, 2, 3, for two horizontal and one vertical components)

ε_{ij} = modal correlation coefficient for modes i and j

R_{p_i} = periodic response or periodic component of a response of mode i

R_{p_j} = periodic response or periodic component of a response of mode j

n = number of modes considered in the combination of modal responses

$$\varepsilon_{ij} = \frac{8\left(\lambda_i \lambda_j f_i f_j\right)^{\frac{1}{2}} \left(\lambda_i f_i + \lambda_j f_j\right) f_i f_j}{\left(f_i^2 - f_j^2\right)^2 + 4\lambda_i \lambda_j f_i f_j \left(f_i^2 + f_j^2\right) + 4\left(\lambda_i^2 + \lambda_j^2\right) f_i^2 f_j^2} \qquad \textbf{(3-2)}$$

where: λ_i and λ_j = modal damping ratios

f_i and f_j = modal frequencies

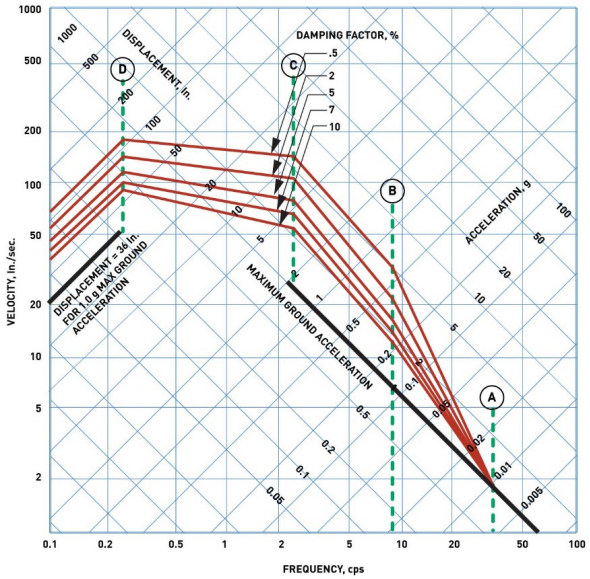

(a) Horizontal design response spectra

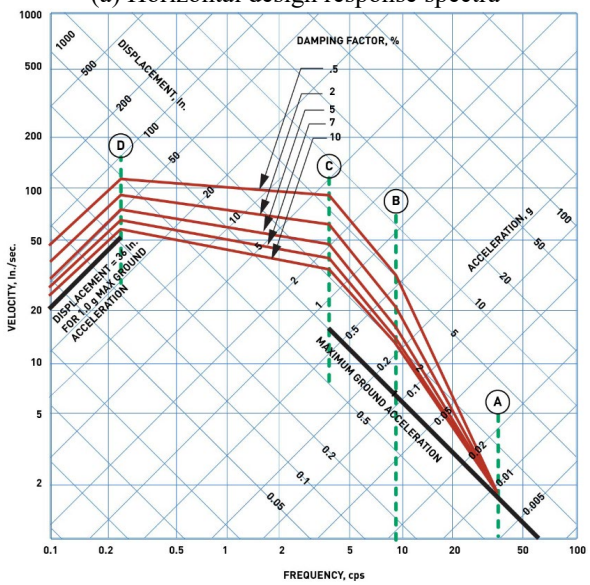

(b) Vertical design response spectra

Figure 3-2 Design response spectra scaled to 1g ground acceleration (RG 1.60)

3.1.3 Considerations for prestressing as demand

As previously mentioned, prestressing as part of the design loads is input as equivalent surface loads acting inwards on the containment, and corresponding to the level of prestressing $X = 1$. Because structural analysis at the preliminary design stage is performed under linear elastic assumptions, higher levels of prestressing as part of the design load can be considered by increasing the load factor for F when superposing the structural responses.

The input effective prestressing in **Table 3-3** is obtained from idealizing the tendon layout as shown in **Figure 3-3** and computing the effective prestressing force per unit length which balances out the design pressure of 54 psi (0.37 MPa). The configuration is divided into 3 parts: shell, dome side and dome apex. Conversion is performed utilizing **Eq. (2-2)**, where the tendon force may be converted to centrifugal forces and vice versa.

Because tendons are located further away from the center point than the inner radius R_i, the converted inward forces act on surface areas greater than the inner surface areas where design pressure is applied. Therefore, the equivalent surface pressures due to prestressing at $X = 1$ are set to be smaller than the design pressure by R_i/R for the shell, and $(R_i/R)^2$ for the dome which has double curvatures along the hoop and meridional direction.

Table 3-4 Analysis assumptions for prestressing at $X = 1$ and $P_a = 54$ psi (0.37 MPa)

Category	Hoop		Meridional
	Shell	Dome	
Number of curvatures	1	2	2
Effective prestress	560 kips/ft (8,173 kN/m)	270 kips/ft (3,940 kN/m)	270 kips/ft (3,940 kN/m)
Radius R	75 ft (22.9 m)	75 ft (22.9 m)	74 ft (22.6 m)
Inward force per unit area	51.84 psi (0.36 MPa)	24.88 psi (0.17 MPa)	25.56 psi (0.18 MPa)
Effective load at inner surface	54.01 psi (0.37 MPa)	27.13 psi (0.19 MPa)	26.77 psi (0.18 MPa)

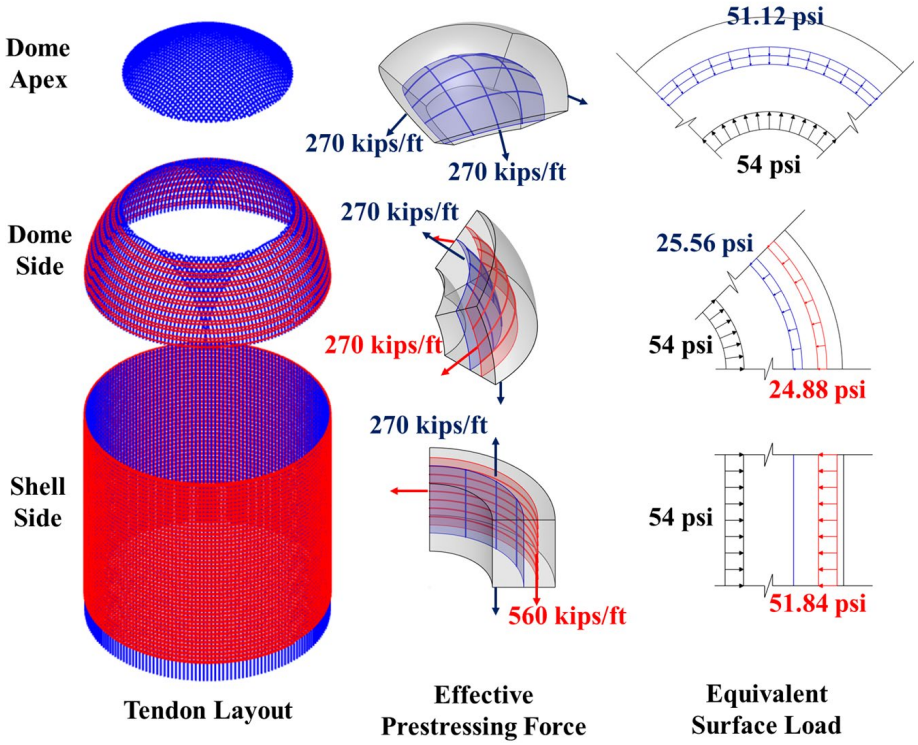

Figure 3-3 Idealization of prestressing along containment
(Conversion: 1 kips/ft = 14.6 kN/m; 1 psi = 7 kPa)

3.2 Analysis results and discussion

3.2.1 Introduction and assumptions

The results of the FEA are illustrated in this subchapter. A strip of meshes is taken along the meridional direction of the containment model to be representative of the structural response. The stress data for the 9 nodes in the thickness direction are integrated, to obtain the forces acting on the containment shown in **Figure 3-4(a)**. Sectional moments in the hoop and meridional directions are obtained by integrating around the geometric centroid, i.e., halfway through the thickness of the containment.

Sectional forces are graphically depicted along the height of the containment inner surface, as shown in **Figure 3-4(b)**. The length from the basemat to the springline (the height at which the shell and dome meet) is 147 ft (44.8 m), while the remainder length up to the dome apex is approximately 113 ft (34.4 m). The meridional direction at the dome corresponds to the direction parallel to the meridional tendons, and the concrete sections are assumed perpendicular to this direction.

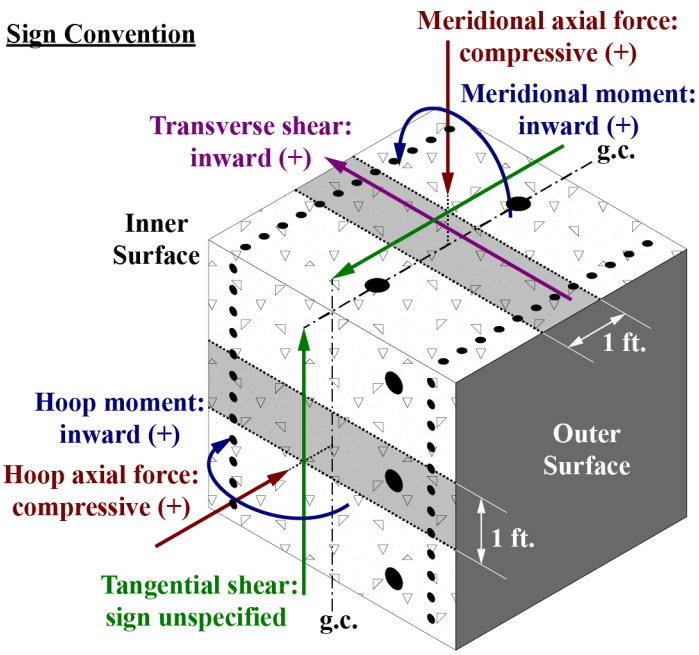

(a) Forces acting at containment sections (Conversion: 1 ft = 0.3 m)

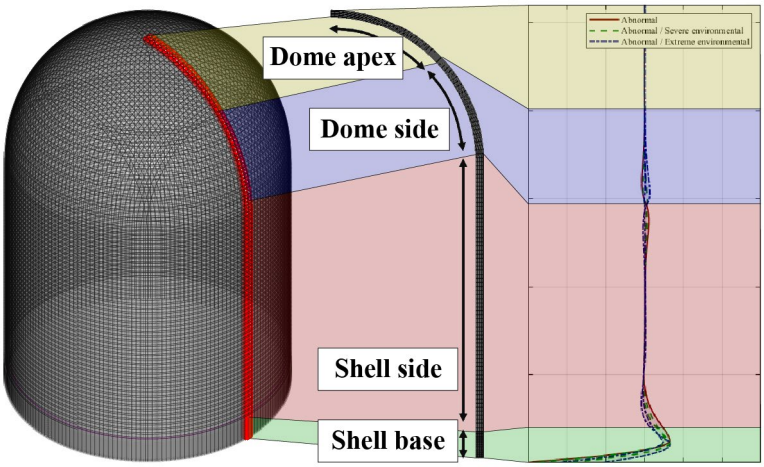

(b) Depiction of sectional force visualization along containment height

Figure 3-4 Graphical depiction of sectional forces acting on PCCVs

3.2.2 Results for factored loads

The sectional forces and moments from each individual design load are obtained and superposed according to the ASME Code load combinations in **Table 3-2**. As previously mentioned in **Section 3.1.3**, levels of prestressing other than X =1 are considered as a structural demand by modifying the load factor value for design load F. The resulting primary forces from factored loads are shown in **Figure 3-5**, for X = 0, 1 and 2. From this figure, the following observations can be made:

- **Figure 3-5(a)** and **(c)**: The hoop and meridional moments are most prominent near the containment base which has a fixed boundary condition, and at the springline where the containment dome and shell converge. Both show similar tendencies in graphs, but the magnitude is larger for meridional moments. An increase in X initially negates the moments resulting from design pressure, but the moment starts to increase after the load has been fully balanced.

- **Figure 3-5(b)** and **(d)**: Axial forces in the meridional direction are governed by Abnormal / severe environmental loads near the containment base, and by Abnormal loads for all other regions. Axial forces in the hoop direction are governed by Abnormal loads throughout the whole containment, being significantly larger at the shell wall. Overall, increasing X decreases the net tensile force, and the concrete sections are kept under compression when X = 2. However, because hoop tendons are only assumed to be placed above 13 ft (4 m) height, hoop sections near the basemat exhibit marginal tensile forces from the factored design pressure load.

- **Figure 3-5(e)**: Transverse shear is most prominent near the basemat and springline, i.e., at geometric discontinuities. Shear force at the springline shows a similar tendency to the bending moment, where an increase in X initially balances out the shear force from design pressure, but increases after that point. On the other hand, near the basemat, the level of prestressing does not balance out shear forces induced by P_a at the basemat. This is due to the inward prestressing load only being input above 13 ft (4 m) height for the structural analysis, whereas the internal pressure was

input for the entirety of the inner surface. Increasing the level of prestressing conversely results in an increase in shear force at the 13 ft (4 m) height.

- **Figure 3-5(f)**: This figure depicts the tangential shear acting on the containment in the in-plane direction. The Abnormal load combination as considered in this analysis does not exert any tangential shear on the containment structure, due to all loads being assumed to be axisymmetric. Seismic loads from OBE or SSE are the design loads which incur tangential shear, and the Abnormal / extreme environmental load corresponding to the assumed SSE governs in this case.

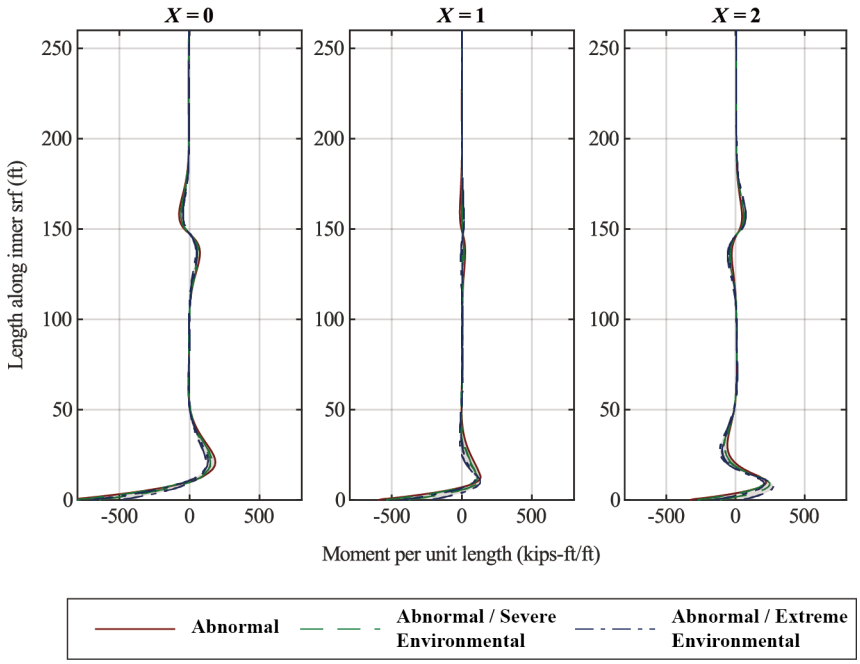

(a) Meridional moment (Conversion: 1 ft = 0.3 m; 1 kips-ft/ft = 4,448 kN-mm/m)

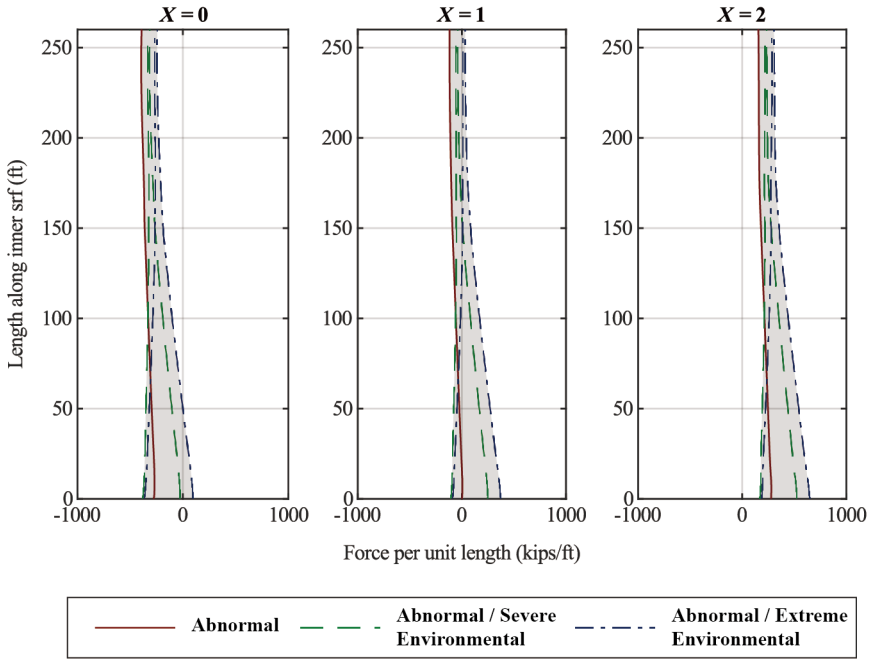

(b) Meridional force (Conversion: 1 ft = 0.3 m; 1 kips/ft = 14.6 kN/m)

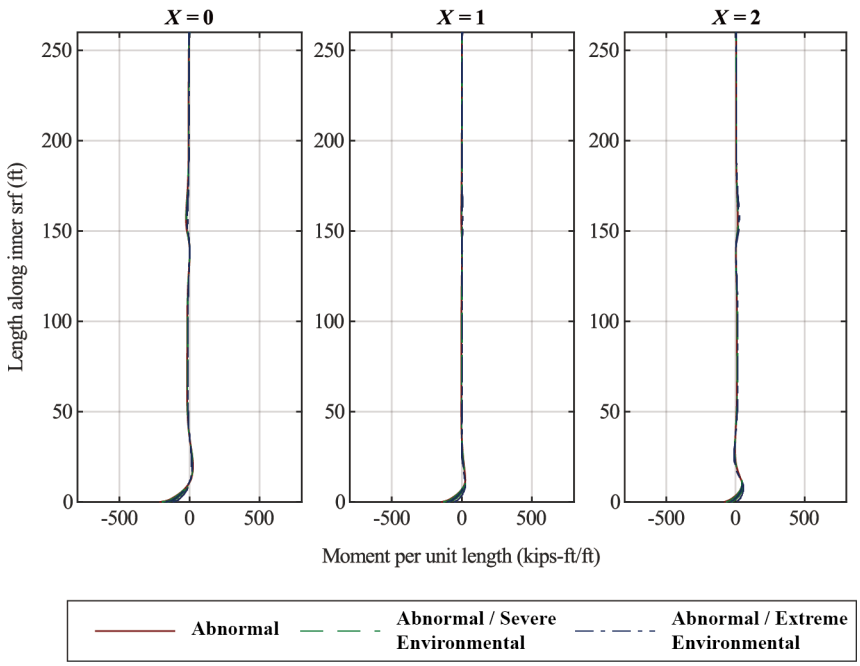

(c) Hoop moment (Conversion: 1 ft = 0.3 m; 1 kips-ft/ft = 4,448 kN-mm/m)

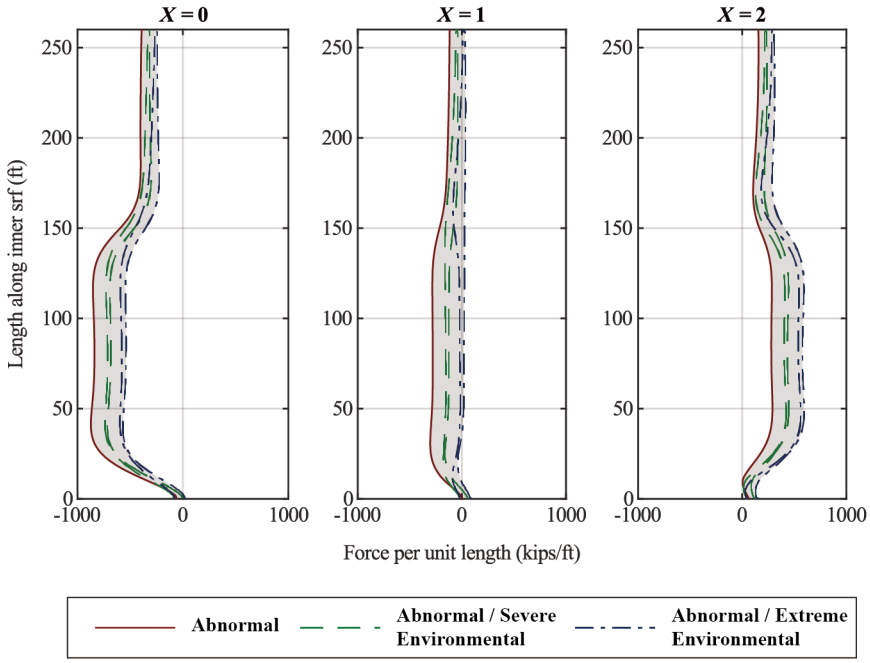

(d) Hoop force (Conversion: 1 ft = 0.3 m; 1 kips/ft = 14.6 kN/m)

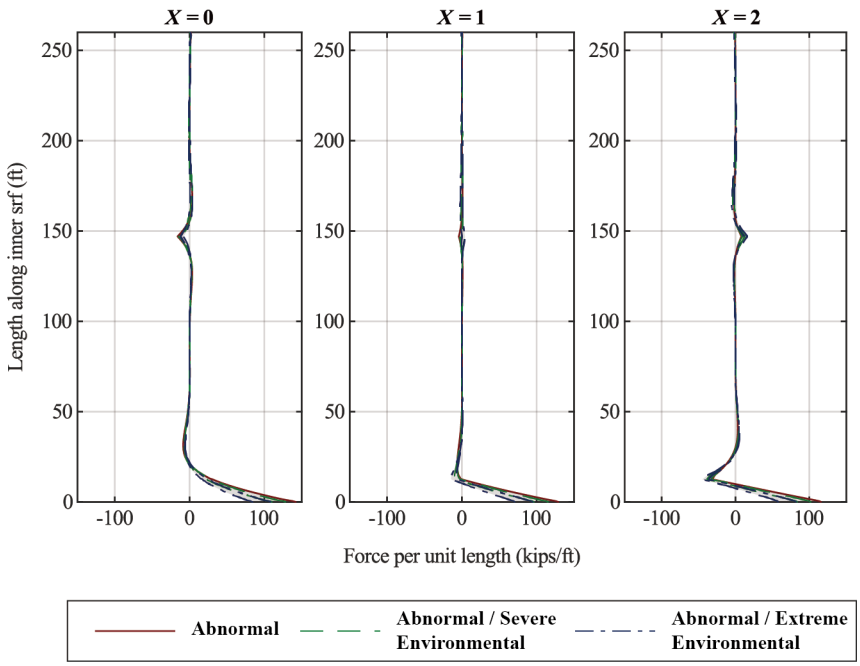

(e) Transverse shear (Conversion: 1 ft = 0.3 m; 1 kips/ft = 14.6 kN/m)

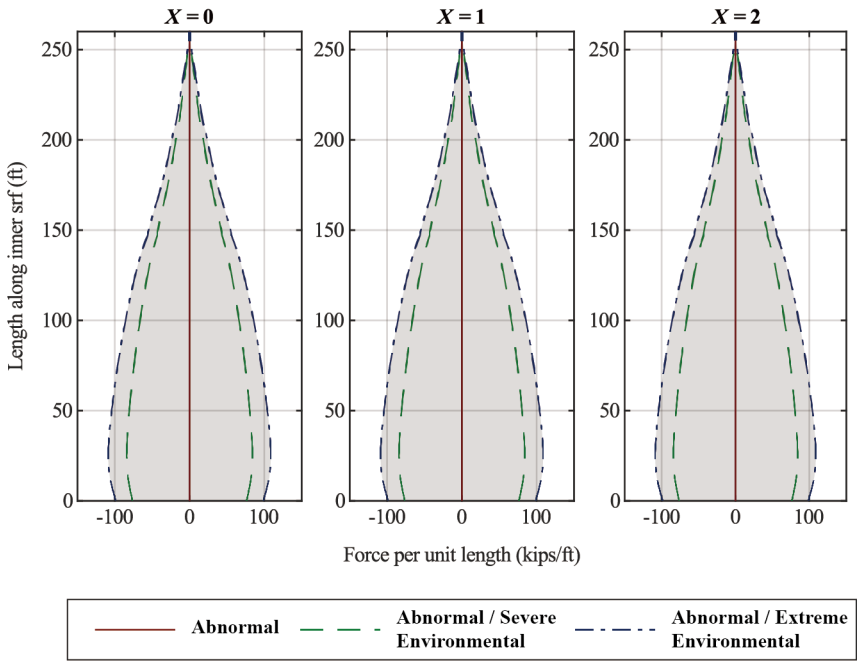

(f) Tangential shear (Conversion: 1 ft = 0.3 m; 1 kips/ft = 14.6 kN/m)

Figure 3-5 Primary factored loads for $X = 0, 1, 2$

Chapter 4. Parametric Study for the Reinforcement Design of Conventional Concrete

4.1 Introduction

This chapter performs reinforcement design according to ASME Code provisions and design methodologies for conventional concrete, taken as class C30/37, across differing levels of prestress. Before proceeding to the design procedure, parameters regarding the prestressing steel and tendon stress distribution are assumed and converted in terms of the level of prestressing.

Based on these assumptions, example P-M interaction curves are generated to confirm the capacity-demand relationship discussed in **Section 2.3.3**, and investigate preferred reinforcing steel layouts. Thereafter, tangential shear design is performed according code provisions. Using the tangential shear design results as lower limits for reinforcing steel area, axial and flexural load design is carried to derive the required volume of reinforcing steel according to level of prestressing.

4.2 Assumptions for post-tensioning

In this chapter, assumptions for prestressing steel sectional properties are given, to provide the necessary information in performing axial and flexural design with prestressing as capacity.

The properties of prestressing steel assumed for this procedure are shown in **Table 4-1**. In order to obtain a reasonable representation of effective prestress f_{se} after short-term and long-term losses, as well as the prestressing steel area A_{ps} which corresponds to $X = 1$, **Eq. (4-1)** from ACI 423 was utilized to obtain tendon stress distributions throughout the meridional and hoop tendons. The

idealized tendon layouts for the meridional and hoop directions are shown in **Figure 4-1(a).**

$$f_x = f_{jack} e^{-(\mu_p \alpha + kx)} \quad \textbf{(4-1)}$$

where: f_x = stress in prestressing steel at distance x from jacking end, ksi (MPa)

f_{jack} = jacking stress, ksi (MPa)

μ_p = curvature friction coefficient

α = total angular change in radians of tendon profile from jacking end

k = wobble friction coefficient, ft^{-1} (m^{-1})

The tendon stress distribution along the half length of the tendons are calculated via **Eq. (4-1)**, and losses shown in **Table 4-2** are subtracted to obtain f_{se} in the meridional and hoop directions. depicted in **Figure 4-1(b)** and **(c)**, respectively.

The effective prestresses f_{se} obtained from these stress distributions at four sections (shell base, shell side, dome side, dome apex) in the hoop and meridional directions are shown in the 3rd column of **Table 4-3**. From these values, the unit prestressing steel area for $X = 1$ are calculated such that the total prestressing force per unit length would be equal to the values given in **Table 3-4**.

Finally, the values in **Table 4-3** are converted to the sectional assumptions for the axial and flexural design, shown in **Figure 4-2**. Thereafter, design will be carried out with prestressing steel considered as capacity, where A_{ps} is multiplied by X for different levels of prestressing.

Table 4-1 Properties of prestressing steel

Tensile strength f_{pu}	270 ksi (1,860 MPa)
Yield strength f_{py}	$0.9f_{pu}$
Maximum jacking stress	$0.8f_{pu}$
Minimum anchor stress	$0.7f_{pu}$
Elastic modulus E_{ps}	28,000 ksi (193 GPa)
Wobble friction factor k	0.0003 ft^{-1} (0.001 m^{-1})
Curvature friction factor μ	0.18
40-year relaxation loss	4% @$0.7f_{pu}$
Creep and shrinkage loss	500 x 10^{-6}

Table 4-2 Assumed short-term and long-term losses

Individual loss	Elastic shortening	3.85 ksi (26.54 MPa)
	Creep and shrinkage	14 ksi (96.53 MPa)
	Relaxation	7.56 ksi (52.12 MPa)
Total loss		25.41 ksi (175.19 MPa)

Table 4-3 Effective prestress and tendon area for $X = 1$

		f_{se}	A_{ps}
Meridional	Shell base	160.47 ksi (1,106 MPa)	1.82 in^2/ft (3,852 mm^2/m)
	Shell side	165.57 ksi (1,142 MPa)	
	Dome side	161.92 ksi (1,116 MPa)	
	Dome apex	134.48 ksi (927 MPa)	
Hoop	Shell base	-	-
	Shell side	149.42 ksi (1,030 MPa)	3.75 in^2/ft (7,938 mm^2/m)
	Dome side	151.77 (1,046 MPa)	1.75 in^2/ft (3,704 mm^2/m)
	Dome apex	-	-

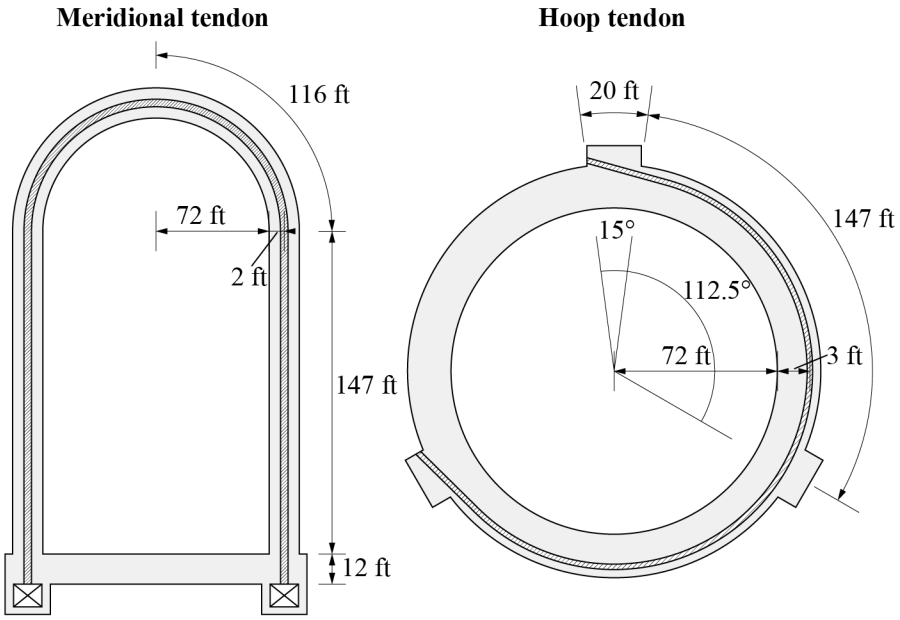

(a) Tendon configuration (Conversion: 1 ft = 0.3 m)

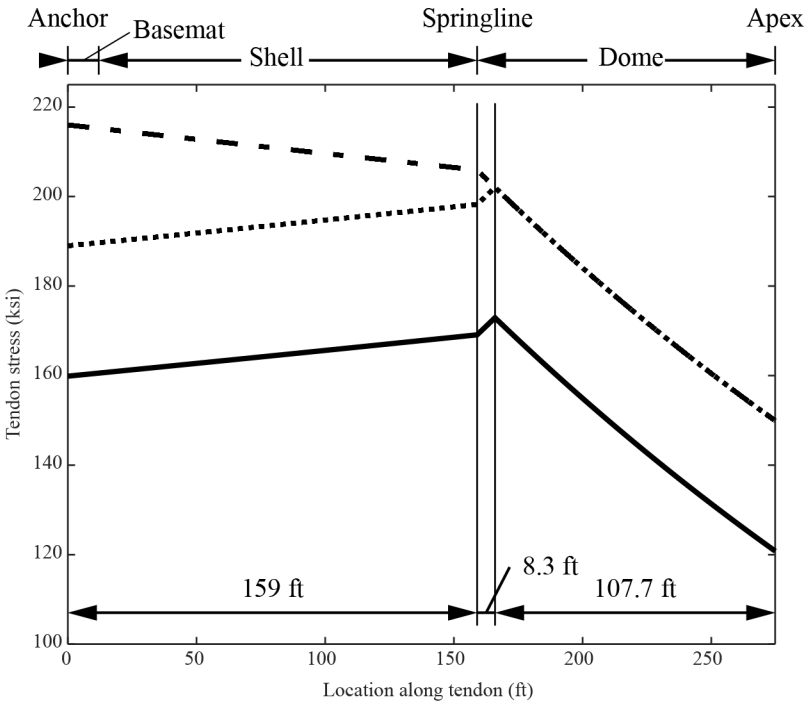

(b) Stress distribution along meridional tendon
(Conversion: 1 ft = 0.3 m; 1 ksi = 7 MPa)

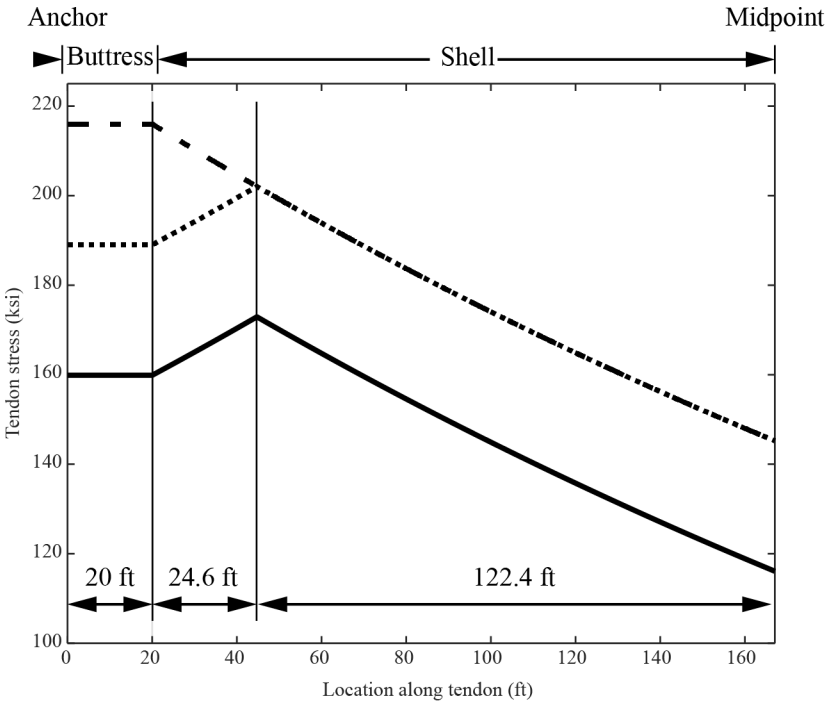

(c) Stress distribution along hoop tendon
(Conversion: 1 ft = 0.3 m; 1 ksi = 7 MPa)

Figure 4-1 Tendon layout and stress distribution

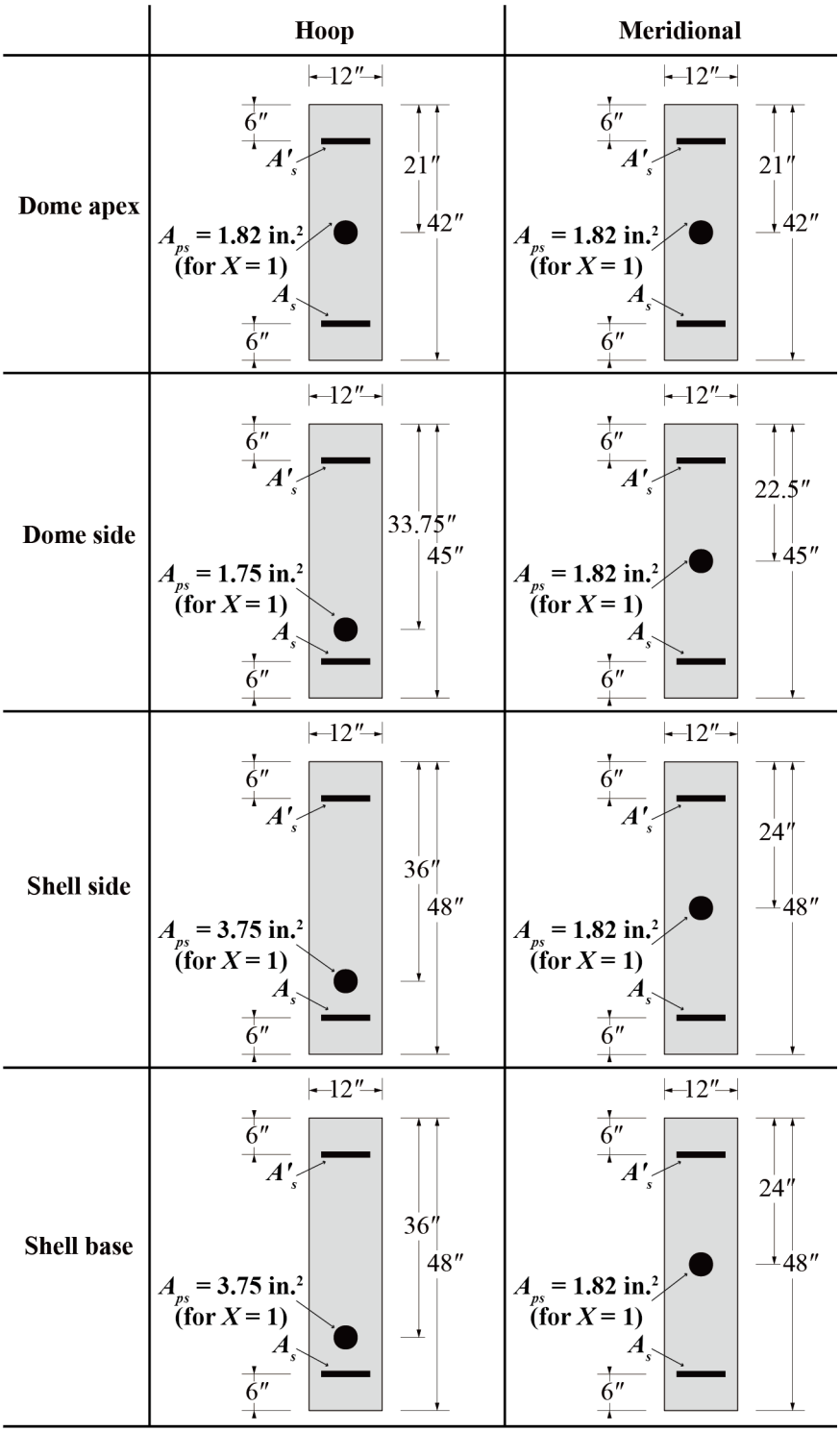

Figure 4-2 Sectional assumptions for P-M curve generation
(Conversion: 1″ = 25.4 mm)

4.3 Axial and flexural design examples

In this section, examples of the axial and flexural design procedure at the shell side are given. The SD methodology for prestressing as demand and capacity outlined in **Section 2.3** are both used to generate P-M curves for concrete class C30/37, with reinforcing steel of f_y = 60 ksi (420 MPa) and E_s = 29,000 ksi (200 GPa). These curves are compared to the data points obtained in **Chapter 3**.

Figure 4-3(a) depicts P-M interaction curves for hoop sections with equal amounts of reinforcement, $A_s = A_s' = 3$ in^2 (1,935 mm^2), on the inner and outer side. In **Figure 4-3(b)**, the P-M curves are generated with all the reinforcing steel concentrated at the inner side. In the left columns, it can self-evidently be observed that when prestressing is considered as demand, an increase in level of prestressing is represented as shifts in data points. On the other hand, in the right columns where prestressing is considered as capacity, the tendencies discussed in **Section 2.3.3** can be observed in detail: the P-M interaction curve is shifted towards the bottom right and the eccentricity is shifted towards the left.

Because of these different tendencies, the preferred reinforcing steel layout at the hoop section is different for these two approaches. When prestressing is considered as demand, a symmetric reinforcing steel layout is preferred, as shown in the left column of **Figure 4-3(a)**. On the other hand, when prestressing is considered as capacity, concentrating the reinforcing steel at the inner side is preferred, as in the right column of **Figure 4-3(b)**.

Figure 4-4 depicts P-M interaction curves for meridional sections. In this case, the tendons are situated around the midpoint of the containment wall thickness, and therefore the eccentricity of membrane tensile stresses would not be shifted by changes in X. It can be seen from comparing the left and right columns of **Figure 4-4** that the relative configurations of the P-M curve and data points largely stay similar. Because of this, the tendency of reinforcing steel requirements at the inner and outer side would not differ much according to the consideration of prestressing.

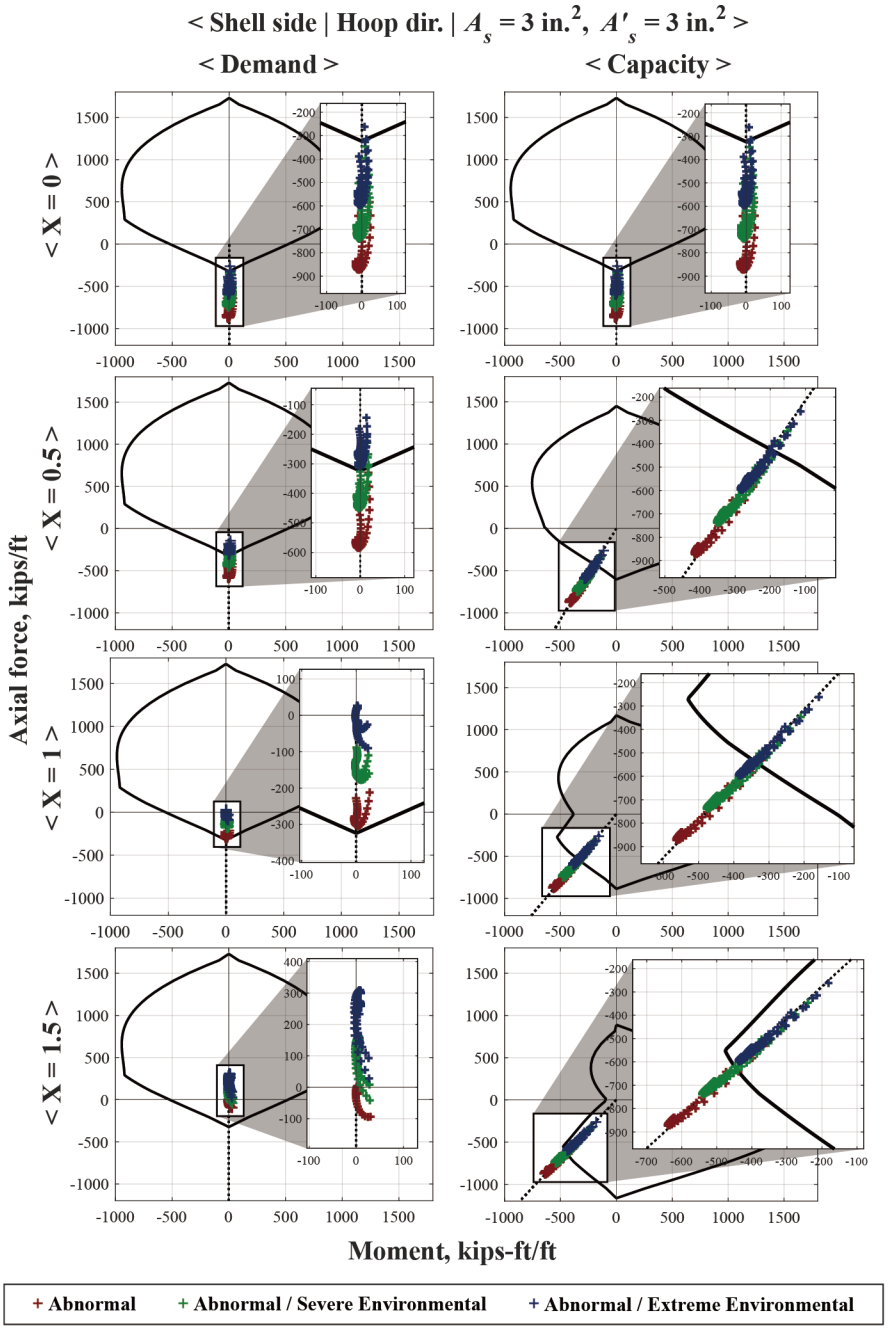

(a) A_s = 3 in^2 (1,935 mm^2) and A_s' = 3 in^2 (1,935 mm^2)
(Conversion: 1 kips/ft = 14.6 kN/m; 1 kips-ft/ft = 4,448 kN-mm/m)

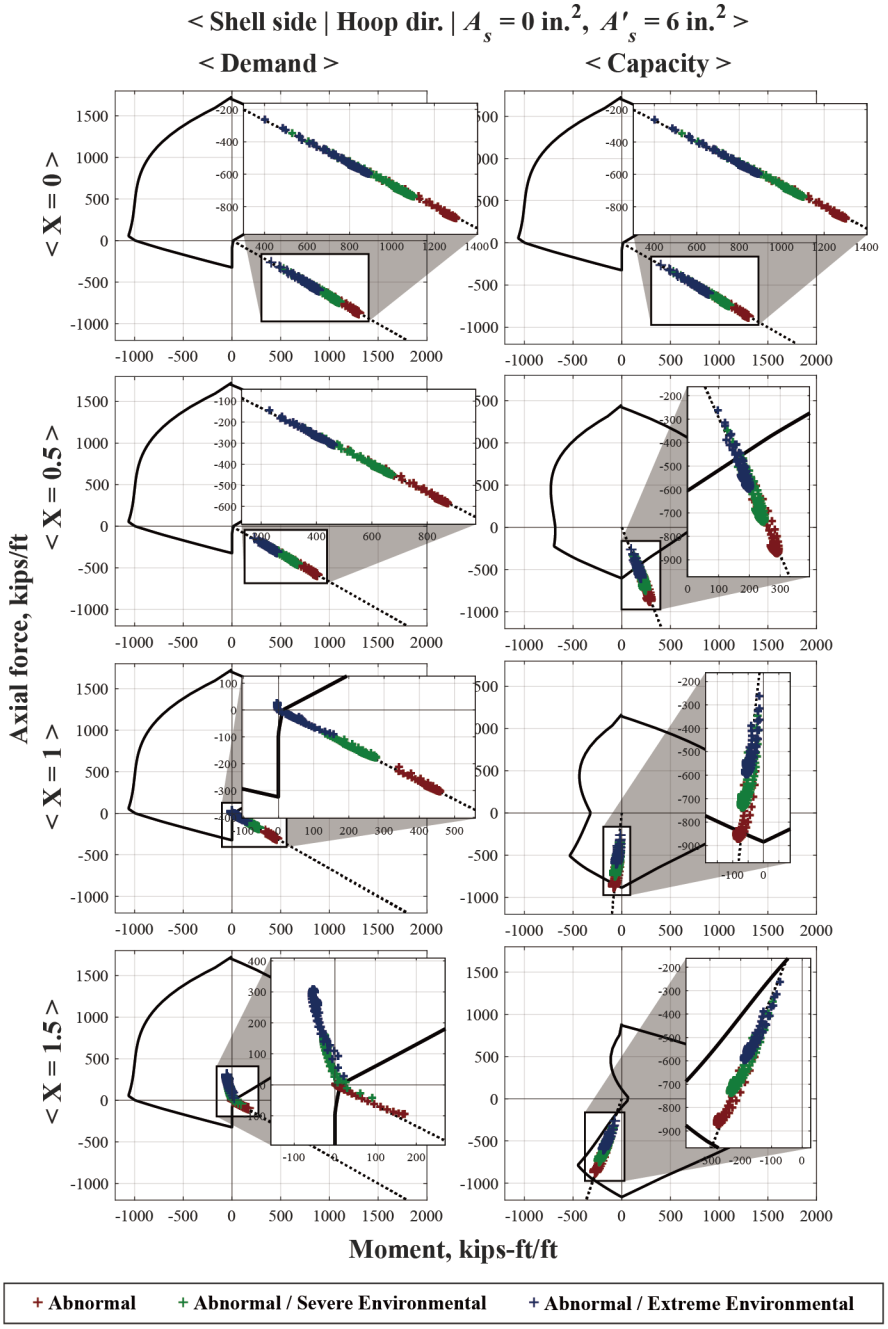

(b) A_s = 0 in^2 and A_s' = 6 in^2 (3,870 mm^2)
(Conversion: 1 kips/ft = 14.6 kN/m; 1 kips-ft/ft = 4,448 kN-mm/m)

Figure 4-3 P-M interaction curves for shell side in hoop direction

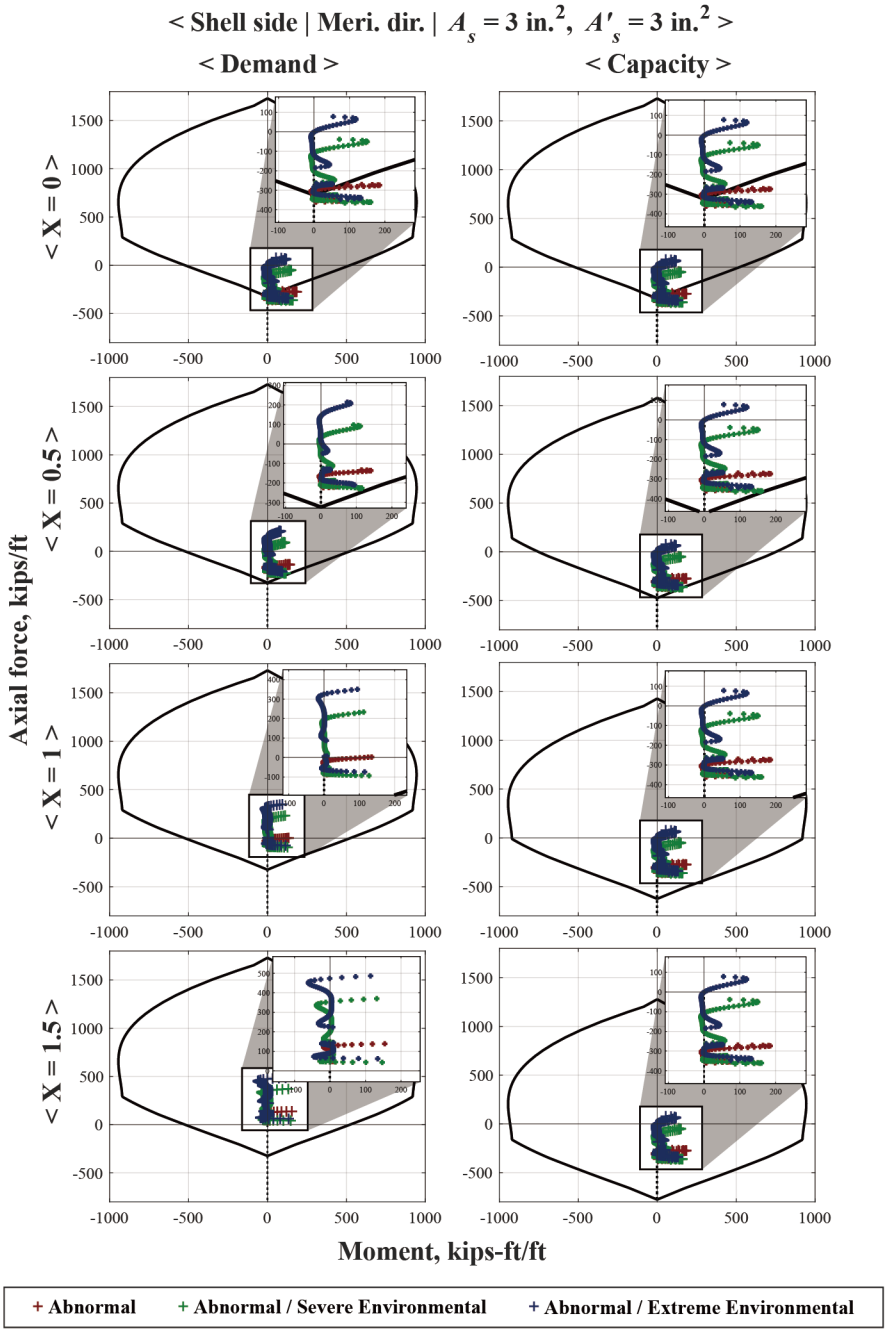

Figure 4-4 P-M interaction curves for shell side in meridional direction for A_s = 3 in^2 (1,935 mm^2) and A_s' = 3 in^2 (1,935 mm^2)
(Conversion: 1 kips/ft = 14.6 kN/m; 1 kips-ft/ft = 4,448 kN-mm/m)

4.4 Parametric study for tangential shear design

In this subchapter, reinforcing steel design for tangential shear load is carried out, to obtain minimum reinforcing area. The design is performed across a unit strip of the PCCV, divided into four segments in two directions (**Figure 4-5**). Because this thesis performs design for the factored primary load criteria, without consideration for secondary effects, **Eq. (2-15)** and **Eq. (2-16)** are used. The tangential shear strength of concrete is ignored and reinforcing steel is assumed resist the tangential shear force entirely. Before performing the design, it should be noted that the tangential shear load is well within the upper limit given by **Eq. (2-19)**, as shown in **Figure 4-6**. Because the tangential shear load does not get affected by level of prestressing, and the compressive strength considered in **Chapter 5** is higher than that of class C30/37, this upper limit will be ignored for the remainder of this thesis.

Figure 4-7 shows the required reinforcing steel areas A_m and A_h, according to the level of prestressing X. The maximum value is taken for the entirety of each segment. A_h is generally greater than A_m at the shell base, shell side and dome side, but is similar for the dome apex. In the meridional direction, the Abnormal / severe environmental loads govern up to the shell side, above which Abnormal loads govern. In the hoop direction, Abnormal / severe environmental loads govern for the shell base, but Abnormal loads govern for the other three segments. Both A_m and A_h decrease as X increases, up to zero.

Figure 4-8 depicts the required rebar volume percentage across the representative unit strip, obtained from performing the tangential shear design process for $X = 0.0 \sim 3.0$. The curve is roughly bilinear, where the effectiveness of increasing X drops off around $X = 1.4$, due to the required rebar volumes at the shell base, dome side and dome apex almost having reached zero. The required rebar volume at the shell side finally reaches zero around $X = 2.0$.

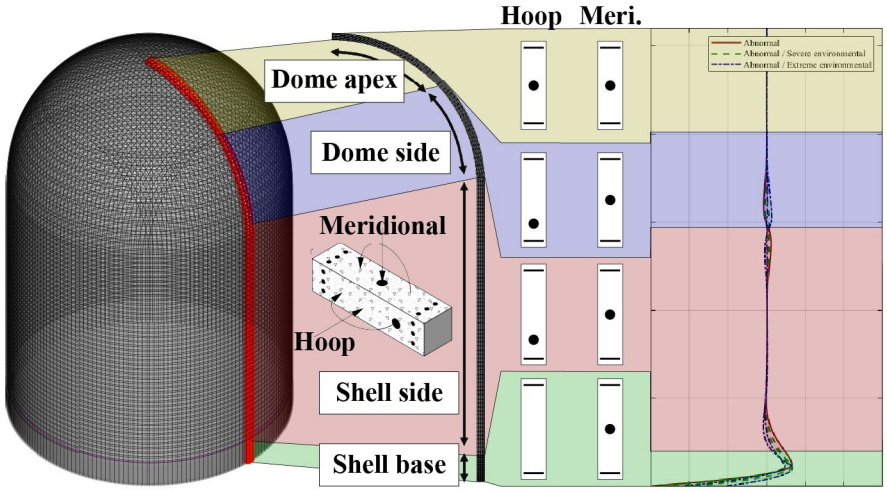

Figure 4-5 Diagram of categories for obtaining rebar area

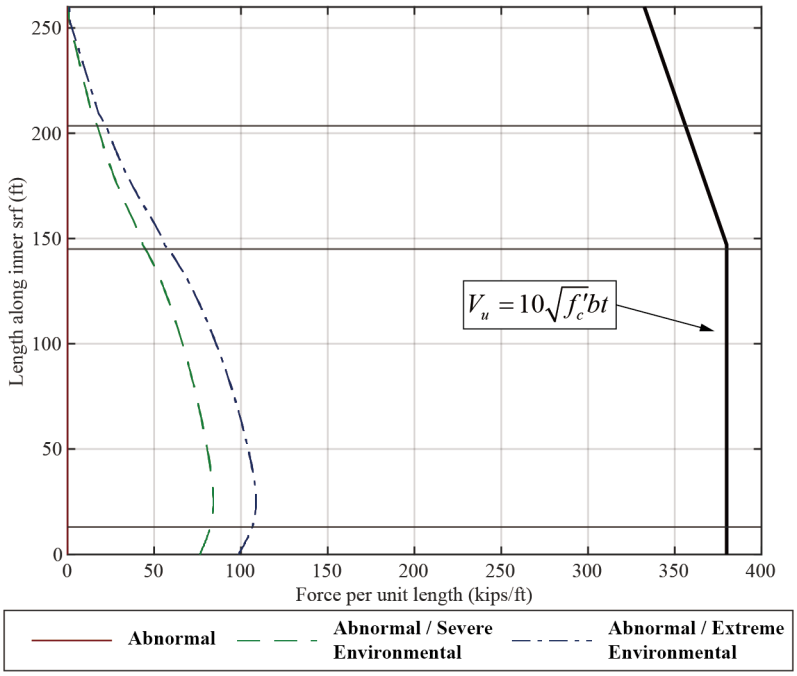

Figure 4-6 Relation between tangential shear load V_u and upper limit
(Conversion: 1 ft = 0.3 m; 1 kips/ft = 14.6 kN/m)

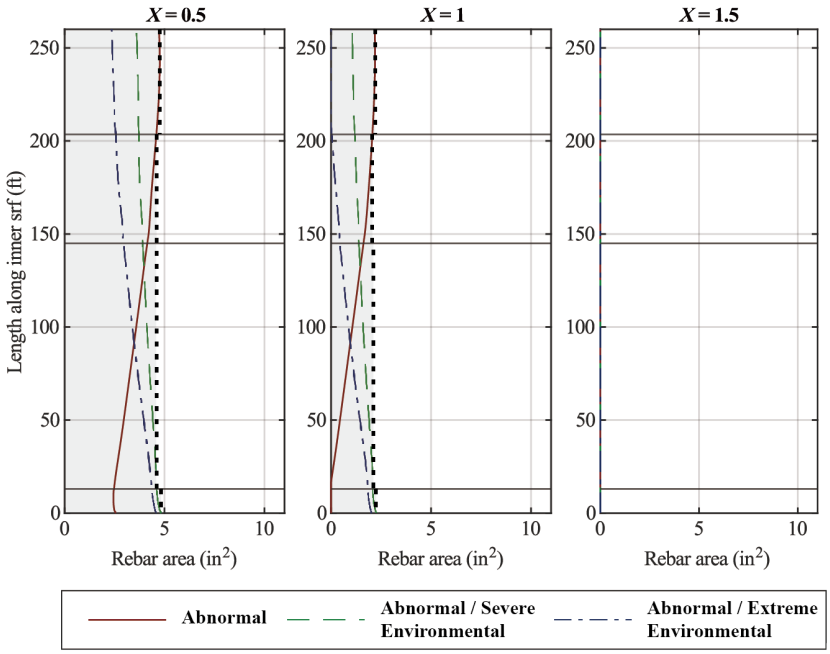

(a) A_m according to level of prestressing
(Conversion: 1 ft = 0.3 m; 1 in. = 25.4 mm)

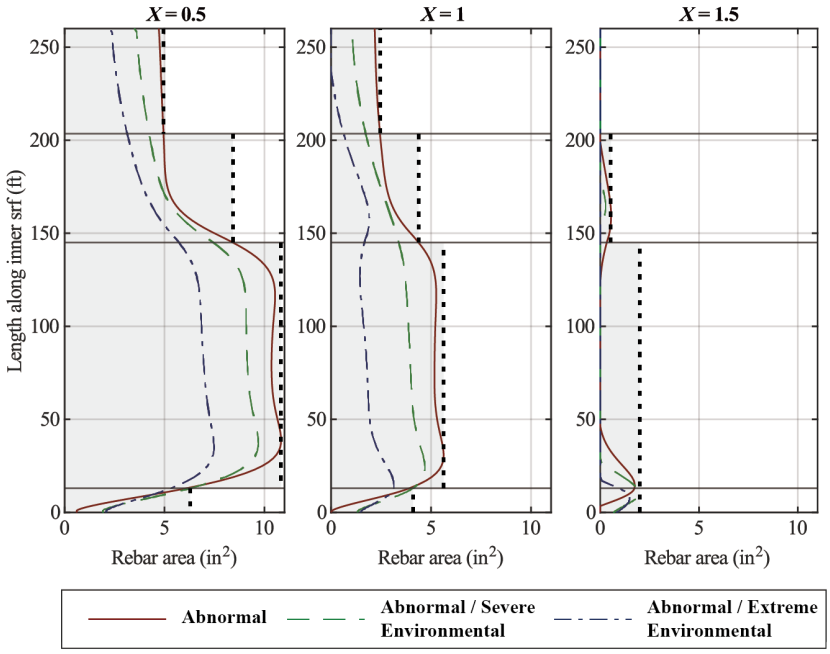

(b) A_h according to level of prestressing
(Conversion: 1 ft = 0.3 m; 1 in. = 25.4 mm)

Figure 4-7 Required reinforcing steel area according to level of prestressing for ASME Code provisions for tangential shear

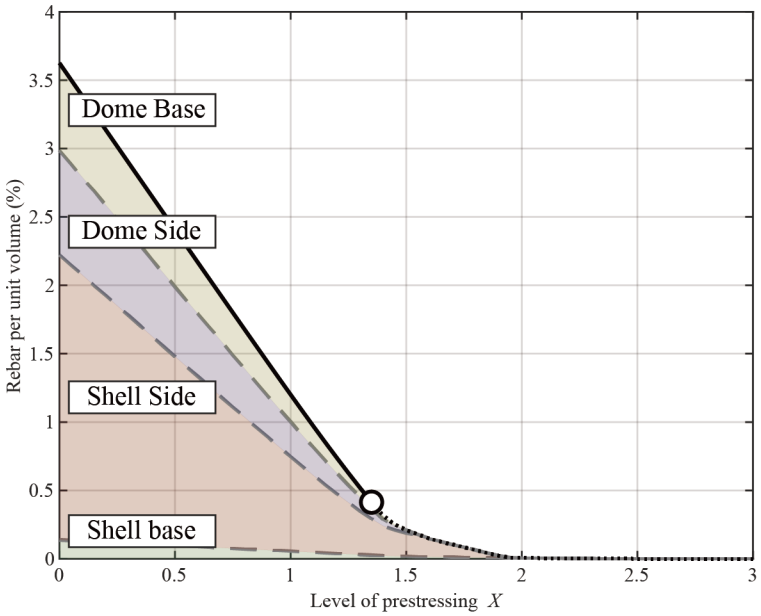

Figure 4-8 Required rebar volume ratio for tangential shear load according to level of prestressing

4.5 Reinforcement design and discussion

4.5.1 Design methodology

This subsection describes the final procedure of reinforcing steel design for concrete class C30/37. In **Section 4.3**, it was discussed that the SD methods considering prestressing as demand or capacity result in different rebar design preferences at the hoop sections. Because of this, axial and flexural design is performed such that the resulting P-M curves from both methods may meet the structural demands from factored design loads. Additionally, the values of A_h and A_m obtained from the previous subchapter are utilized as lower bounds in obtaining the required reinforcing steel area via axial and flexural design, which not only derives the combined design results, but also greatly reduces computational load.

To achieve this, a MATLAB code is devised where the level of prestressing X is increased in increments of 0.05, and for each value of X, the reinforcing steel area at the inner and outer layers are also increased individually in increments of 0.05 in^2 (32 mm^2), up to 20.0 in^2 (12,900 mm^2). All combinations of reinforcing areas A_s and A_s' are checked, and the minimum value of $A_s + A_s'$ is obtained such that the P-M curves for prestressing as demand and capacity both encompass the respective data points.

As presented earlier in **Figure 4-5**, the containment is divided into four segments with a unit width of 1 ft (305 mm), and the incremental process mentioned above is repeated for all segments until X reaches a value of 3.0. The maximum allowable X for concrete class C30/37 is 1.34 (**Table 2-6**), but the level of prestressing is extended up to 3.0 for comparison with high performance concrete in the following chapter. **Figure 4-9** presents a schematic diagram depicting this overall design procedure.

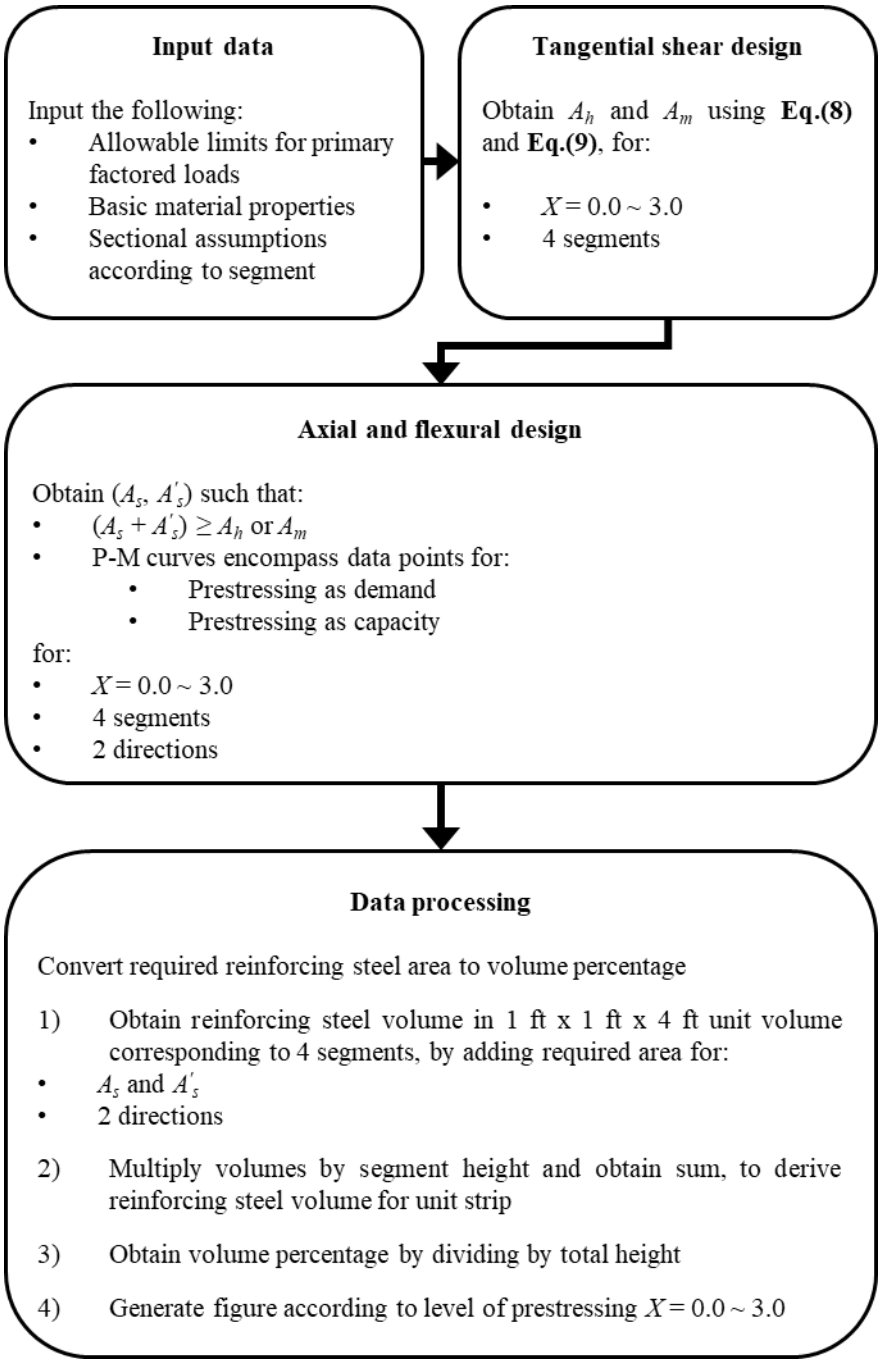

Figure 4-9 Diagram of obtaining required reinforcing steel volume using MATLAB code (Conversion: 1 ft = 0.3 m)

4.5.2 Results and discussion

The results of reinforcing design for the assumed concrete C30/37 are depicted in **Figure 4-10**. **Figure 4-10(a)** shows that the reinforcing requirements for axial/flexural loads govern over those for tangential shear. Requirements for tangential shear and axial/flexural load with prestressing as demand show a similar trend, with the latter being slightly more conservative. On the other hand, design results for axial/flexural load with prestressing as capacity show a distinctly different trend from the other design methods, where the rebar requirements start to increase after $X = 1.6$, and become the sole governing factor after the requirements for the other approaches have reached zero.

This trend can be attributed to the configuration of the P-M curve in the hoop direction, as displayed in **Figure 2-12**. Because the eccentricity of governing loads and the P-M curves are shifted in separate direction according to the level of prestressing, the P-M curves after a certain threshold will not be able to encompass membrane tensile stress without increasing the reinforcing steel volume to compensate. However, this threshold occurs around $X = 1.6$, which is above $X_{max} = 1.34$ (**Figure 4-10(b)**). In practice, the allowable compressive stress limits would prevent levels of prestressing to reach such conditions.

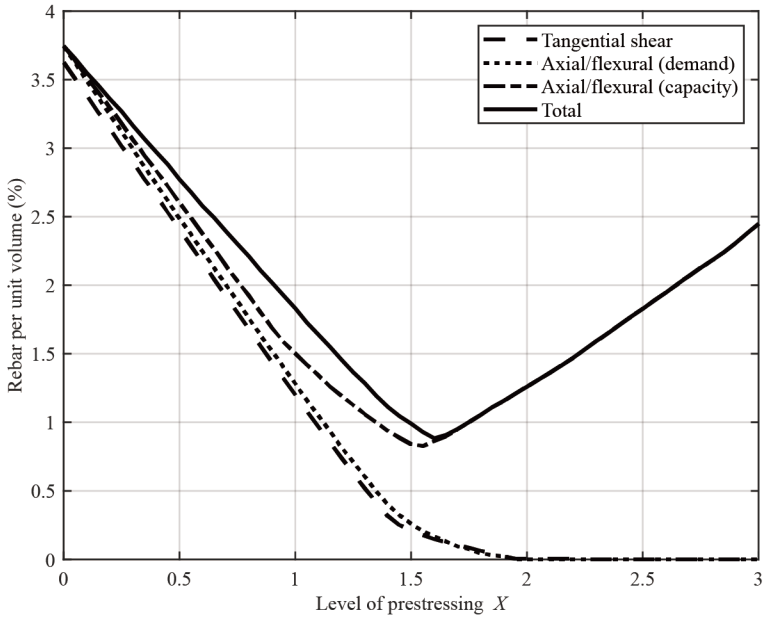

(a) Required rebar volume ratio according to individual design method

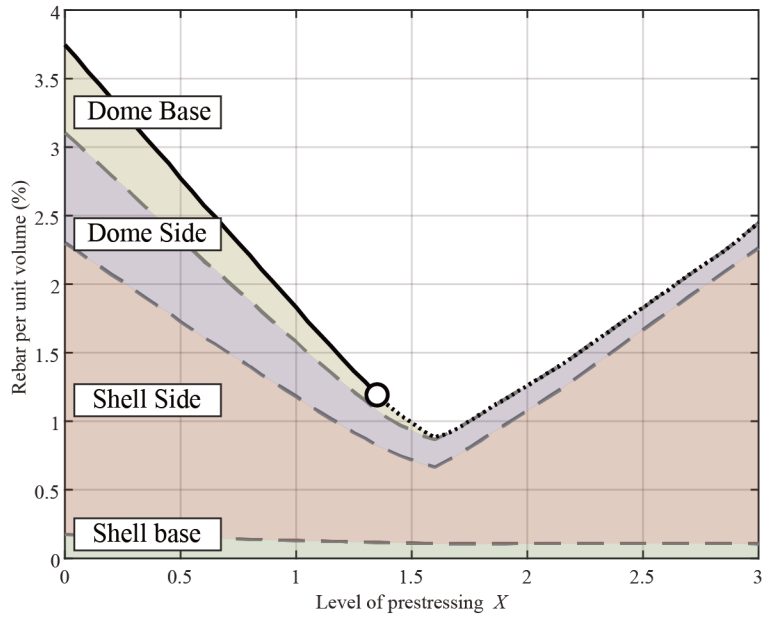

(b) Average rebar volume ratio and contribution of parts

Figure 4-10 Required rebar volume ratio for C30/37 according to level of prestressing

Chapter 5. Parametric Study for the Design of High Performance Concrete

5.1 Introduction

This chapter takes the reinforcement design methodology outlined in **Chapter 4** and expands upon it for high performance concrete, keeping in mind the potential benefits explained in **Section 2.5**. To provide comparative studies for the generation of P-M curves in axial and flexural design, alternate parameters of α_1, β_1 and $\varepsilon_{c,allow}$ are derived according to the compressive constitutive laws of high performance concrete. The properties of concrete classes C40/50 through C90/105 are taken from Eurocode 2, while those of UHPC are taken from NF P18-710.

In the case of UHPC, the effects of including the tensile strength of concrete in computing sectional capacity are also investigated. A representative tensile stress-strain relationship is obtained from the design laws for thick members in NF P18-710, with the indicative values given in Annex T. Similar to Bae (2011), the tensile law is idealized as a rectangular tensile stress block.

Once the compressive and tensile stress blocks for high performance concrete are defined, the SD methodology is analogously performed as a parametric study according to the concrete strength and implementation of concrete tensile strength, and considering prestressing as both demand and capacity. The characteristics of the P-M curves in relation to the data points are investigated. Finally, the resulting rebar requirements from the axial and flexural design methodology are obtained, and the results are discussed.

5.2 Constitutive laws of high performance concrete

This subchapter details the material properties assumed for the high performance concrete, as well as their constitutive laws and idealizations for the SD methodology. The material properties of concrete are shown in **Table 5-1** and **Table 5-2**, taken from Eurocode 2 and NF P18-710, respectively.

The compressive laws for normal to high strength concrete are obtained from **Eq. (5-1)**, which is modified from Eurocode to include the characteristic compressive strength f_{ck} instead of the design compressive strength f_{cd}, and multiplied by 0.85 as an additional factor of safety. The characteristic strength is used because the conservatism from implementing partial safety factor γ_c and coefficient for long-term effects α_{cc} are already accounted for with the multiplication of 0.85 and the additional membrane stress allowable limit of $0.75f_c^{'}$ under primary factored load criteria.

This equation accounts for the tendency of high strength concrete to exhibit stress-strain relation close to linear elastic up to the peak stress, and at higher corresponding strains. However, the concrete thereafter shows more brittle behavior as the strength increases (ACI Committee 363, 2010).

$$\begin{gathered} f_c = 0.85 f_{ck}\left[1-\left(1-\frac{\varepsilon_c}{\varepsilon_{c2}}\right)^n\right] \quad \text{for } 0 \le \varepsilon_c \le \varepsilon_{c2} \\ f_c = 0.85 f_{ck} \quad \text{for } \varepsilon_{c2} \le \varepsilon_c \le \varepsilon_{cu2} \\ f_c \le 0.75 f_{ck} \end{gathered} \tag{5-1}$$

where: n = exponent according to **Table 5-1**
ε_{c2} = strain at peak strength
ε_{cu2} = ultimate strain

The compressive law for UHPC is derived from the linear design relation given in NF P18-710, using indicative properties which are also provided in the Annex T of said guideline. For the compressive side, the stress-strain relation is taken to be linear elastic up to the characteristic compressive strength. As with the normal to high strength concretes, f_{ck} is taken in place of f_{cd}, and relation is multiplied by 0.85. The assumed compressive stress-strain relationships for concrete classes C30/37, C60/75, C90/105 and UHPC are

shown in **Figure 5-1(a)**, where the straight lines depict the design laws up to $0.75f_c'$, considered in the primary factored load criteria.

Using the resulting compressive constitutive laws for concrete, compiled in the parameters α_1, β_1 and $\varepsilon_{c,allow}$, are recalculated to obtain stress blocks which are computationally equivalent to the design stress-strain relationship. The resulting values are given in **Table 2-1**, where α_1 and β_1 do not deviate far from those for normal strength concrete, only decreasing from 0.60 to 0.56 and from 0.70 to 0.67, respectively.

In the case of the tensile law, the design stress-strain relationship is first obtained from NF P18-710 equations for thick members of class T2. Due to the lack of ASME Code allowable limits on the consideration of concrete tensile strength, a partial safety factor of 1.2 taken from Annex U of NF P18-710. The resulting tensile stress-strain relationship is depicted in **Figure 5-1(b)**.

Thereafter, an idealized tensile stress block is defined according to the tensile stress f_{ct} = 134.54 psi (0.93 MPa). This value of f_{ct} is taken at the reinforcing steel tensile strain limit of $2\varepsilon_y$ for the primary factored load criteria. This approach was taken because: 1) the computational load in performing axial and flexural design would be reduced, 2) the P-M curve obtained from the stress block provides conservative results compared to those obtained from the discretized layer analysis using the exact design law, and 3) the P-M curve is expressed as a closed curve without knots forming due to a descending stress-strain relationship.

Table 5-1 Concrete material properties taken from Eurocode 2

	C30/37	C60/75	C90/105
f_{ck}	4,350 psi (30 MPa)	8,700 psi (60 MPa)	13,050 psi (90 psi)
n	2	1.6	1.4
ε_{c2}	0.0020	0.0023	0.0026
ε_{cu2}	0.0035	0.0029	0.0026

Table 5-2 UHPC material properties taken from NF P18-710

Young's modulus E_{cm}	8,000 ksi (552 GPa)
Characteristic compressive strength f_{ck}	25,400 psi (175 MPa)
Mean compressive strength f_{cm}	28,300 psi (195 MPa)
Characteristic tensile limit of elasticity $f_{ctk,el}$	1,235 psi (8.52 MPa)
Mean tensile limit of elasticity $f_{ctm,el}$	1,450 psi (10 MPa)
Characteristic post-cracking strength f_{ctfk}	1,160 psi (8 MPa)
Mean post-cracking strength f_{ctfm}	1,230 psi (8.48 MPa)
Global fiber orientation factor K_{global}	1.25
Local fiber orientation factor K_{local}	1.75
Length L_f	0.63 in. (16 mm)
Partial safety factor γ_{cf}	1.2

Table 5-3 Parameters for concrete stress block under primary factored load criteria

	C30/37	C60/75	C90/105	UHPC
α_1	0.60	0.60	0.59	0.56
β_1	0.70	0.70	0.69	0.67
$\varepsilon_{c,allow}$	0.0013	0.0017	0.0020	0.0028

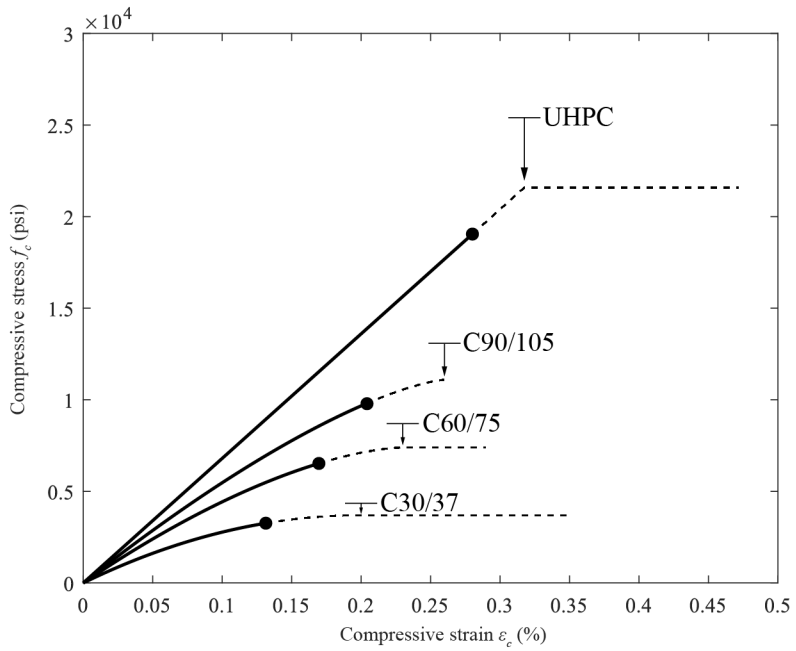

(a) Assumed compressive law of concrete (Conversion: 1,000 psi = 7 MPa)

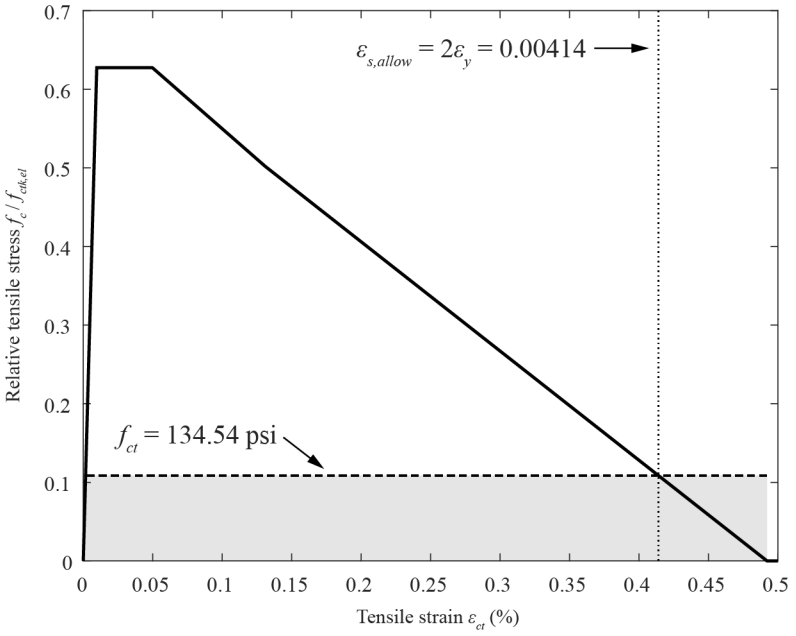

(b) Assumed tensile law of UHPC (Conversion: 1,000 psi = 7 MPa)

Figure 5-1 Constitutive law for concrete under primary factored load criteria

5.3 Axial and flexural design example for UHPC

This section constructs a P-M interaction curve from the assumptions made for UHPC in **Section 5.2**, and investigates the effects of implementing concrete tensile strength in axial and flexural design. **Figure 5-2** compares the P-M interaction curves for hoops sections at the shell side generated from: compressive stress block (dashed line), compressive and tensile stress block (solid line) and actual design law (dash-single dotted line).

The implementation of tensile stress blocks results in enlarged P-M curves at the tensile side, which is expected from the additional consideration of tensile capacity, and would hold true for meridional sections as well. Also, the eccentricity of the membrane tensile stress is shifted towards the center, because the added contribution of concrete at the tensile plastic state balances the p.c. towards the g.c. Both of these changes are beneficial to the reduction of reinforcing steel requirements, in terms of the positional capacity-demand relationship.

Comparing the P-M curves generated from the tensile stress block approach to those obtained from the exact design law, it can be seen that the method used for this thesis is notably more conservative than the ASD approach. This level of conservatism could be optimized in future studies; nonetheless, adopting a constant stress block instead of a trapezoidal design law avoids the problem of having knots at the bottom of the P-M curve which occur due to the descending slope of the tensile law.

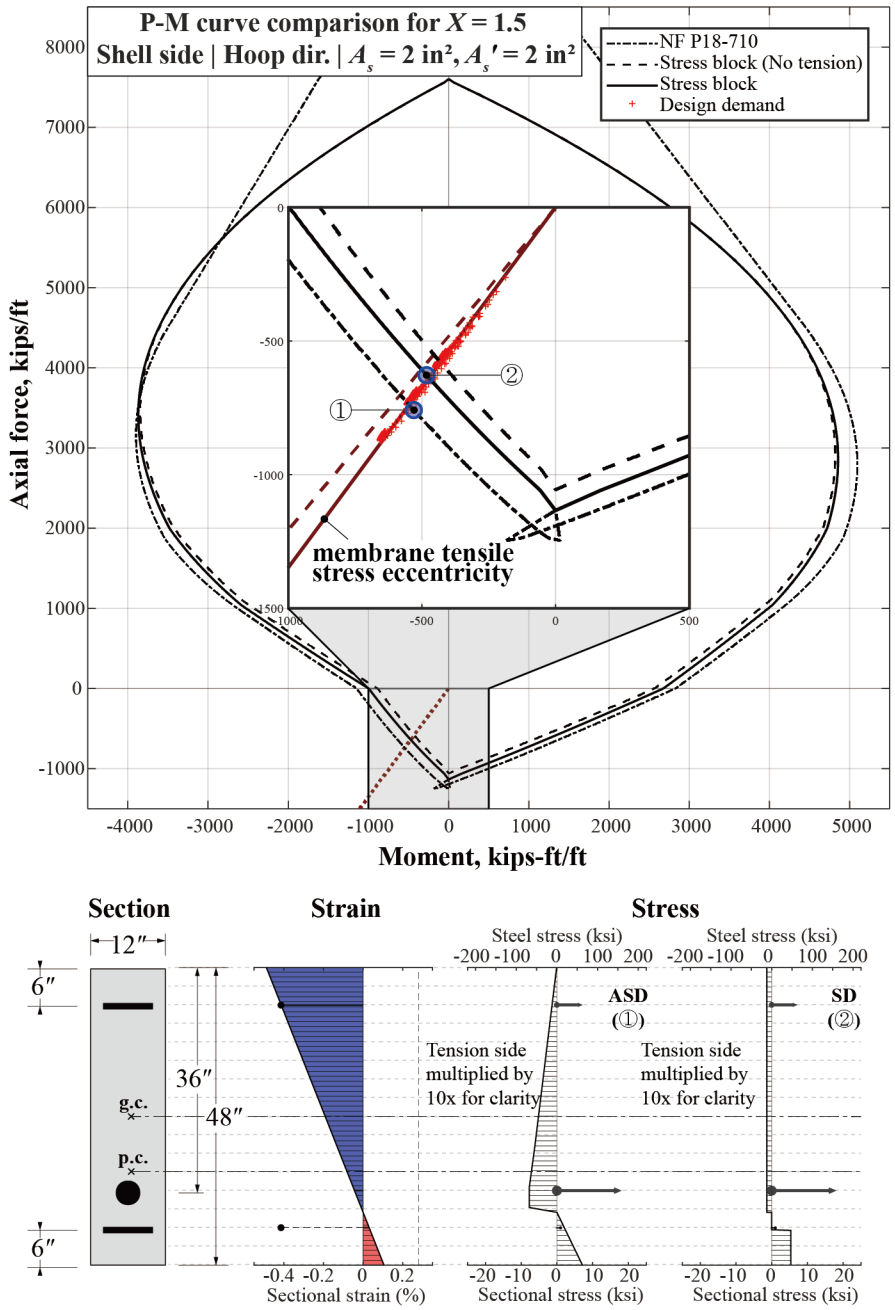

Figure 5-2 Generation of P-M curves for UHPC
(Conversion: 1 kips/ft = 14.6 kN/m; 1 kips-ft/ft = 4,448 kN-mm/m;
1 ksi = 7 MPa; 1″ = 25.4 mm)

5.4 Design results and discussion

In this subchapter, the reinforcement design methodology from **Chapter 4** is utilized for concrete classes C30/37 through C90/105, as well as UHPC with and without consideration of its tensile strength. The results are summed up in **Figure 5-6**.

It can first be observed in **Figure 5-6(a)** that, similar to the requirements for C30/37, concrete classes up to C60/75 show the tendency of rebar requirements increasing at high levels of prestress. However, the maximum levels of prestressing set by **Eq. (2-20)** sufficiently contain X below the threshold for this trend to occur, so this would not be a design concern. In the case of concrete classes C70/85, C80/95 and C90/105, as well as UHPC, this increase in reinforcing steel requirements does not occur at $X < 3.0$.

The curves for required rebar volume at higher strength instead show a roughly bilinear trend, when kept under the limits of **Table 2-6**. The slope decreases after a level of prestressing is increased to around $X = 1.5$, after which the efficacy drops off. The requirements for $X < 1.5$ are almost identical regardless of the concrete strength, because the observation of concrete strength contributing to structural capacity in **Figure 2-12** is only valid when paired with a meaningful level of prestressing.

The slopes of the required volume curves for $X > 1.5$ show minor differences according to the concrete strength. C60/75 exhibits a nearly flat slope, whereas the slope gets steeper for C90/105 and UHPC. However, while this does result in rebar requirements being lessened at high levels of prestressing for concretes of higher strength, the difference is minimal.

On the other hand, the consideration of the tensile strength of UHPC does indeed result in a meaningful reduction in rebar. The overall configuration of the rebar requirement curve is similar to that of the curve without consideration for concrete tensile strength, but shifted to the bottom left. The curve also shows a bilinear trend, in this case the slope dropping off when $X = 1.4$. The maximum efficacy of requirement reduction is also reached at $X = 1.4$, but the reduction at $X = 1.5 \sim 3.0$ is nonetheless similar to the reduction at the typical domain of $X = 1.0 \sim 1.5$.

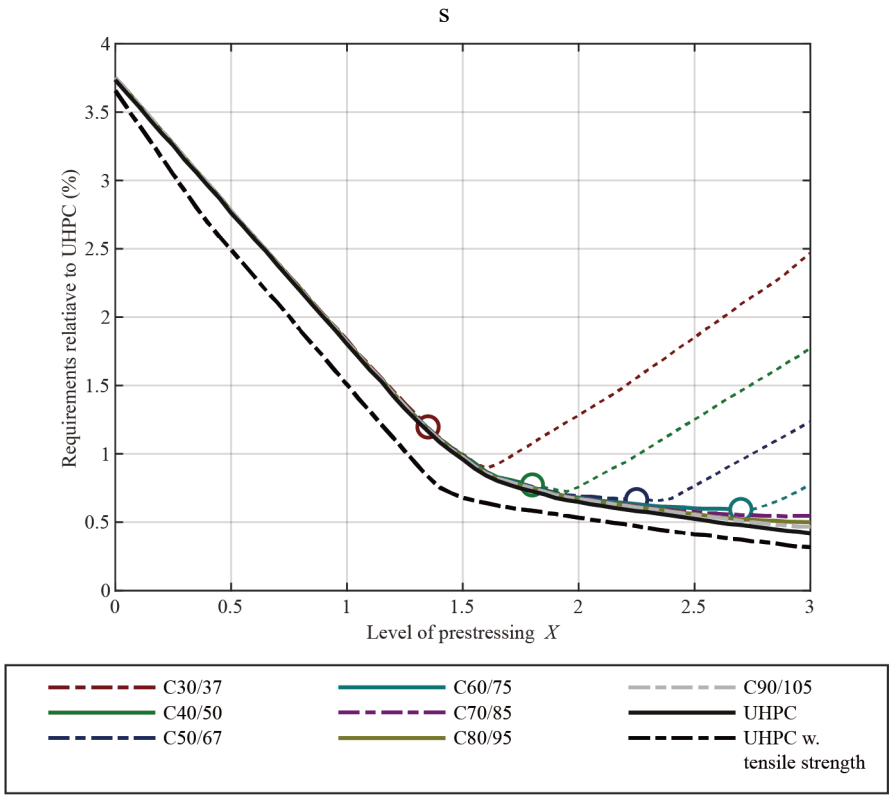

(a) Requirements according to level of prestressing

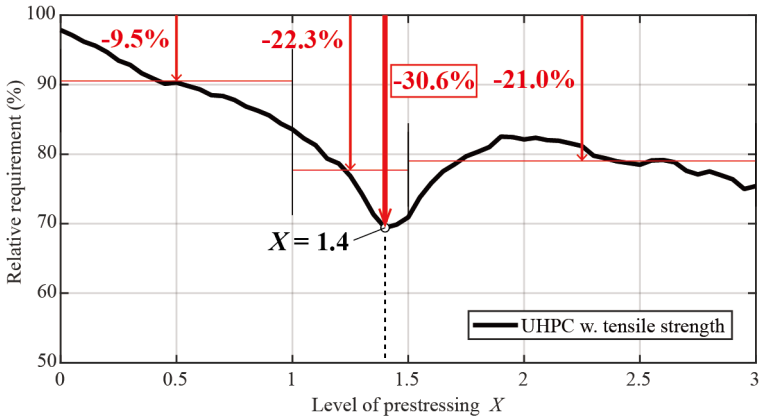

(b) Requirement reduction from consideration of concrete tensile strength

Figure 5-3 Required reinforcing steel volumes across different concrete classes

Chapter 6. Conclusion

In this study, a reinforcement design methodology of ASME Code utilizing ultimate strength design was reviewed, and structural analysis was performed for a hemispherical dome type PCCV for primary factored loads. Thereafter, a parametric study was carried out investigating the rebar requirements according to the level of prestressing, and additionally accounting for prestressing as part of structural capacity. This design process was analogously repeated for high performance concrete with modified parameters derived from their mechanical properties and constitutive laws, along with considerations for the concrete tensile strength in terms of UHPC. The results can be summed up as follows:

1) ASME Code adopts the allowable stress design method in principle, but also allows for an ultimate strength design approach in Code Case N-850 where parameters are modified to satisfy allowable stress and strain limits. This method provides a way to visually represent the structural demand and capacity via data points and P-M interaction curves with lessened computational loads, and was used as the baseline for this thesis' design approach. An additional method of constructing P-M curves with prestressing as capacity was implemented, as to consider the effects of hoop tendon eccentricity. However, the code does not provide guidance on the implementation of high performance cementitious materials. Thus, the higher strength concrete classes and respective material properties were taken from Eurocode 2, and those for UHPC were taken from French guideline NF P18-710 which complements Eurocode 2.

2) Finite element analysis was performed on a concrete containment model with concrete class C30/37, and the sectional forces from the primary factored load criteria defined in ASME Code were obtained. P-M interaction curves were generated by considering prestressing either as demand or capacity. The two methods resulted in different rebar design preferences for the hoop sections on the shell side: considering prestressing as demands favors having similar reinforcing steel areas at the inner and

outer layer, while considering prestressing as capacity favors focusing reinforcing steel at the inner layer. For meridional sections on the shell side the rebar design preferences are similar.

3) Reinforcement design was performed for concrete class C30/37, where tangential shear design and axial/flexural load design with prestressing as demand or capacity were carried out sequentially. The average required rebar percentage per unit volume was obtained according to the level of prestressing. It was observed that both methods of considering prestressing contributed to overall more conservative requirements before $X = 1.7$, after which the requirements for prestressing as capacity governs the reinforcement design. Also, when X is greater than 1.6 the rebar requirements start to increase according to the level of prestressing, due to the concrete strength of C30/37 being insufficient. Because the low compressive strength already limits the maximum level of prestressing to $X = 1.34$, this is not an actual design concern.

4) The reinforcement design process of **Chapter 4** was analogously performed for concrete classes C30/37 through C90/105 as well as UHPC, using alternate parameters to obtain the equivalent concrete stress blocks. In the case of UHPC, the effects of considering its tensile strength was also implemented by utilizing a tensile stress block. Generally, increasing the compressive strength did not have a notable impact on rebar requirements aside from allowing for higher levels of prestressing. The requirements for prestressing as demand were not affected, while requirements for prestressing as capacity were alleviated at high levels of prestressing but on a marginal level. On the other hand, implementing the tensile strength of UHPC with stress blocks notably reduced the required reinforcing steel volume, even at levels of prestressing higher than $X = 1.5$.

In conclusion, higher compressive strength benefits reinforcing steel design indirectly by allowing for higher levels of prestressing, while marginally contributing in terms of directly structural capacity. On the other hand, considering the tensile strength of concrete resulted in direct and meaningful reductions of the required rebar volume according to the level of prestressing. However, as this thesis focuses on the Design Basis Domain and uses simplified assumptions for the sake of parametric study, there is a need for more research

utilizing detailed containment models with nonlinear assumptions, as well as performing probabilistic risk assessments for items such as ultimate pressure capacity or seismic hazards.

References

1. Abrishami, H., Tcherner, J., Barre, F., Borgerhoff, M., Bumann, U., Calonius, K., Courtois, A., Debattista, J.-M., Gallitre, E., and Isard, C. (2015). *Bonded or unbonded technologies for nuclear reactor prestressed concrete containments*. Organisation for Economic Co-Operation and Development, Paris, France, 227 pp.

2. ACI Committee 239. (2018). *Ultra-High Performance Concrete: An Emerging Technology Report (ACI 239R-18)*, American Concrete Institute, Farmington Hills, MI, 21 pp.

3. ACI Committee 349. (2014). *Code Requirements for Nuclear Safety-Related Concrete Structures and Commentary* (*ACI 349-13)*, American Concrete Institute, Farmington Hills, MI, 196 pp.

4. ACI Committee 363. (2010). *Report on High-Strength Concrete (ACI 363R-10)*, American Concrete Institute, Farmington Hills, MI, 65 pp.

5. ACI Committee 423. (2016). *Guide to Estimating Prestress Losses (ACI 423.10-16)*, American Concrete Institute, Farmington Hills, MI, 64 pp.

6. AFCEN. (2012). *EPR Technical Code for Civil Works (ETC-C 2012)*, French Society for Design, Paris, France, 509 pp.

7. AFNOR. (2016). *National addition to Eurocode 2—Design of Concrete Structures: Specifique Rules for Ultra-High Performance Fibre-Reinforced Concrete (UHPFRC) (NF P18-710)*, French Standardization Association, La Plaine Saint-Denis, France, 136 pp.

8. Alqam, M., Alkhairi, F. M., and Naaman, A. E. (2021). “Stress at Ultimate in Prestressed Unbonded Tendons: Assessment of Code Equations and Recommendation,” *ACI Structural Journal*, Vol. 118, No. 5, pp. 177-187.

9. Atominform. (1989). *Standard on Design of Reinforced Concrete Structures of Safety Important NPP Buildings (PNAE G-10-007-89)*, Central Research and Development Institute for Management, Economics and Information of the Ministry of Nuclear Industry of the Russian Federation, Moscow, Russia, 41 pp. (in Russian)

10. Bae, S. (2011). "Concrete Stress Block Method for Nuclear Containments," *ACI Structural Journal*, Vol. 108, No. 5, pp. 434-443.

11. Boverket. (1970). *Swedish Building Regulations Supplement (SBN-S 25:21)*, Swedish National Board of Housing, Building and Planning, Karlskrona, Sweden. (in Swedish)

12. CEN. (2004). *Eurocode 2: Design of Concrete Structures - Part 1-1: General Rules and Rules for Buildings*, European Committee for Standardization, Brussels, Belgium, 225 pp.

13. Choi, J. (2018). *Investigating Delamination Behavior of Curved Post-tensioned Concrete Structures* [Doctoral dissertation, University of Texas at Austin], University of Texas Libraries, https://repositories.lib.utexas.edu/handle/2152/82547.

14. Choun, Y.-S. and Park, H.-K. (2015). "Containment Performance Evaluation of Prestressed Concrete Containment Vessels with Fiber Reinforcement," *Nuclear Engineering and Technology*, Vol. 47, No. 7, pp. 884-894.

15. Christou, P., Michael, A., and Neofytou, Z. (2011). "Development of Interaction Diagrams for RC Sections Confined with CFRP Composites," *WIT Transactions on Modelling and Simulation*, Vol. 51, pp. 385-396.

16. CSA. (1993). *Design Requirements for Concrete Containment Structures for CANDU Nuclear Power Plants (CAN/CSA N287.3-93)*, Canadian Standard Association, Toronto, Canada, 59 pp.

17. CSA. (2008). *Material Requirements for Concrete Containment Structures for CANDU Nuclear Power Plants (CAN/CSA N287.2-08)*, Canadian Standard Association, Toronto, Canada, 64 pp.

18. CSA. (2019). *Canadian Highway Bridge Design Code (CSA S6:19)*, Canadian Standard Association, Toronto, Canada.

19. El-Helou, R. G., & Graybeal, B. A. (2019). "The Ultra Girder: A Design Concept for a 300-foot Single Span Prestressed Ultra-High Performance Concrete Bridge Girder," *Second International Interactive Symposium on UHPC*, Vol. 2, No. 1, New York, NY.

20. El-Helou, R. G., & Graybeal, B. A. (2022). "Flexural Behavior and Design of Ultrahigh-Performance Concrete Beams," *Journal of Structural Engineering*, Vol. 148, No. 4, 04022013.

21. Fafitis, A. (2001). "Interaction Surfaces of Reinforced-Concrete Sections in Biaxial Bending," *Journal of Structural Engineering*, Vol. 127, No. 7, pp. 840-846.

22. Freidin, C. and Krichevsky, A. (2002). "Prestressed concrete containment of nuclear power station with PWR," *Nuclear Engineering and Design*, Vol. 214, No. 3, pp. 173-182.

23. Gosstroy. (1985). *Concrete and Reinforced Concrete Structures (SNiP 2.03.01-84)*, State Committee for Construction, Moscow, Russia. (in Russian)

24. "Hanbit Nuclear Power Plant," *Wikipedia*, Wikimedia Foundation, last modified 30 Dec 2021, https://en.wikipedia.org/w/index.php?title=Hanbit_Nuclear_Power_Plant&oldid=1062771838

25. IAEA. (2021). *IAEA Safety Standards SSG-67 "Seismic Design for Nuclear Installations"*, International Atomic Energy Agency, Vienna, Austria, 65 pp.

26. Interatomenergo. (1989). *Standard on Design of Safety Important NPP Buildings (NTD tema 08.05.50.)*, Moscow, Russia. (in Russian)

27. Jeon, S.-J. and Jin, B.-M. (2016). "Improvement of Impact-Resistance of a Nuclear Containment Building Using Fiber Reinforced Concrete," *Nuclear Engineering and Design*, Vol. 304, pp. 139-150.

28. Johnson, T. E., Hovis, B., Jovall, O., and Munshi, J. (2016). *Commentary on Article CC-3000 Design*, ASME Press, New York, NY, 120 pp.

29. Joint ACI-ASME Committee 359. (2011). *BPVC Section III - Division 2 - Code for Concrete Containments (ACI 359)*. ASME Press, New York, NY, 240 pp.

30. Joint ACI-ASME Committee 359. (2019). *BPVC Section III - Division 2 - Code for Concrete Containments (ACI 359)*. ASME Press, New York, NY, 240 pp.

31. JSME. (2011). *Rules on Concrete Containment Vessels for Nuclear Power Plants (JSME S NE1-2011)*, Japan Society of Mechanical Engineers, Tokyo, Japan, 230 pp. (in Japanese)

32. Kim, T.-H. (2011). "Parametric Study on the PM Interaction Diagram of Hollow Prestressed Concrete Bridge Columns," *Journal of the Earthquake Engineering Society of Korea*, Vol. 15, No. 6, pp. 1-10. (in Korean)

33. Moon, I.-H., Kim, T. Y., and Jeong, J. A. (2010). "Design and Durability of Concrete Structure in Nuclear Power Plant," *Magazine of the Korea Concrete Institute*, Vol. 22, No. 6, pp. 44-49. (in Korean)

34. Naaman, A. E. (2004). *Prestressed concrete analysis and design: Fundamentals*, 2nd ed. Techno Press 3000, Sarasota, FL, ISBN 978-0-9674-9391-6.

35. Nuclear Industry Standards of the People's Republic of China. (1995). *The Design Code for the Prestressed Concrete Containment of the PWR NPP (EJ/T 926-95)*, China. (in Chinese)

36. "Nuclear Power Plant | Definition, Principles & Components," Nuclear Power, retrieved 30 May 2022, https://www.nuclear-power.com/nuclear-power-plant/

37. NRC. (2007). *Standard Review Plan for the Review of Safety Analysis Reports for Nuclear Power Plants: LWR Edition (NUREG-0800) - Introduction*, U.S. Nuclear Regulatory Commission, Rockville, Maryland. 9 pp.

38. NRC. (2007). *Regulatory Guide 1.61 Damping Values for Seismic Design of Nuclear Power Plants (RG 1.61)*, U.S. Nuclear Regulatory Commission, Rockville, Maryland. 12 pp.

39. NRC. (2012). *Regulatory Guide 1.92 Combining Modal Responses and Spatial Components in Seismic Response Analysis (RG 1.92)*, U.S. Nuclear Regulatory Commission, Rockville, Maryland. 24 pp.

40. NRC. (2014). *Regulatory Guide 1.60 Design Response Spectra for Seismic Design of Nuclear Power Plants (RG 1.60)*, U.S. Nuclear Regulatory Commission, Rockville, Maryland. 13 pp.

41. NRC. (2015). *Standard Review Plan for the Review of Safety Analysis Reports for Nuclear Power Plants: LWR Edition (NUREG-0800) - 19.0 Probabilistic Risk Assessment and Severe Accident Evaluation for New Reactors*. U.S. Nuclear Regulatory Commission, Rockville, Maryland. 41 pp.

42. OECD/NEA/CSNI. (2015). *Bonded or Unbonded Technologies for Nuclear Reactor Prestressed Concrete Containments*, Committee on the Safety of Nuclear Installations, Paris, France, 227 pp.

43. "Q&A: EU Taxonomy Complementary Climate Delegated Act," European Commission, last modified 2 Feb 2022, https://ec.europa.eu/commission/presscorner/detail/en/QANDA_22_712

44. Salmons, J. R. and McLaughlin, D. G. (1982). "Design Charts for Proportioning Rectangular Prestressed Concrete Columns," *PCI Journal*, Vol. 27, No. 1, pp. 120-143.

45. Sandia National Laboratories. (2003). *Overpressurization Test of a 1:4-Scale Prestressed Concrete Containment Vessel Model (NUREG/CR-6810)*, U.S. Nuclear Regulatory Commission, Washington, D.C., VA, 606 pp.

46. Seo, D. W. and Noh, H. C. (2013). "Aircraft Impact Analysis of Steel Fiber Reinforced Containment Building," *Journal of the Computational Structural Engineering Institute of Korea*, Vol. 26, No. 2, pp. 157-164. (in Korean)

47. SIA. (2016). *Recommendation: Ultra-High Performance Fibre-Reinforced Cement-based Composites (UHPFRC) Construction Material, Dimensioning, and Application (SIA 2052)*, Swiss Society of Engineers and Architects, Lausanne, Switzerland, 48 pp. (in German)

48. Vägverket. (1949). *State Concrete Regulations*, Swedish Road Administration, Borlänge, Sweden. (in Swedish)

49. Vägverket. (1965). *Bridge Construction Manual*, Swedish Road Administration, Borlänge, Sweden. (in Swedish)

50. Valaparambil, S. S., Sivan, P. P., and Gomez, S. M. (2014). "A MATLAB Program for Interaction Curves of Prestressed Concrete Columns with High Tensile Steel Bars," *IOSR Journal of Mechanical and Civil Engineering*, Vol. 11, pp. 35-39

51. Wang, C.-K. and Salmon, C. G. (1998). *Reinforced Concrete Design*, Wiley, Hoboken, NJ, ISBN 978-0-4713-6422-1.

52. Whitney, C. S. (1937). "Design of Reinforced Concrete Members Under Flexure or Combined Flexure and Direct Compression," *Proceedings of the American Concrete Institute*, Vol. 33, No. 3, pp. 483-498.

53. Willam, K., Xi, Y., Naus, D. J., and Graves, H. L. (2013). *A Review of the Effects of Radiation on Microstructure and Properties of Concretes Used in Nuclear Power Plants (NUREG/CR-7171)*, U.S. Nuclear Regulatory Commission, Washington, D.C., VA, 131 pp.

54. Yang, K.-H. and Kang, T. H.-K. (2011). "Equivalent Strain Distribution Factor for Unbonded Tendon Stress at Ultimate," *ACI Structural Journal*, Vol. 107, No. 2, pp. 217-226.

55. Zheng, Z., Sun, Y., Pan, X., Su, C., and Kong, J. (2022). "The Optimum Steel Fiber Reinforcement for Prestressed Concrete Containment Under Internal Pressure," *Nuclear Engineering and Technology*, Vol. 54, No. 6, pp. 2156-2172.

국 문 초 록

고성능 콘크리트를 적용한 포스트텐션 원전 격납건물의 설계방법론에 대한 매개변수 연구

프리스트레스트 콘크리트 격납건물은 원자력시설의 심층방어개념의 일환으로서, 방사성 물질의 유출을 방지하는 최종적 방벽으로 기능하여 원자력 발전소의 안전을 담보한다. 그러나 해외 등지에서 콘크리트 격납건물 건설 시 비용초과와 공기지연이 대두되어 국제시장에서 강재 격납용기와 비교하여 경쟁력을 확보하기 위해서는 콘크리트 격납건물 설계의 질적인 향상이 요구되고 있다.

본 연구는 콘크리트 격납건물에 고성능 콘크리트 적용 시 요구철근량이 감축되어, 시공성이 개선되고 철근 과밀화를 최소화할 수 있는 가능성에 주목한다. 우선, 콘크리트의 압축성능 개선으로 보다 높은 프리스트레스력을 가할 수 있는 경우, 설계사고 시에도 콘크리트가 압축 상태에 있도록 설계할 수 있다. 또한, 초고성능콘크리트(UHPC)와 같이 강섬유가 보강된 시멘트 복합재료의 경우 유의미한 인장연성거동을 보이며, 이러한 특성을 반영한 설계지침이 전세계적으로 개발되는 중이다.

현재는 콘크리트 격납건물에 고성능 콘크리트를 적용하는 방안과 관련된 기술기준 및 설계지침 마련과 관련된 연구가 미흡한 실정이다. 따라서 본 논문은 고성능 콘크리트의 도입과 관련된

요건에 따른 요구철근량의 변화를 평가하는 매개변수 연구를 수행하였다. 가정된 매개변수는 프리스트레스력의 크기, 설계에서 프리스트레스력 도입방식, 콘크리트 압축강도, 그리고 콘크리트의 인장강도 고려여부이다. 구조해석은 상용 유한요소해석 프로그램을 사용하여 ASME BPVC III-2에서 정의하는 1차 계수하중에 대해 수행되었다. 휨과 축하중에 대한 설계는 ASME Code Case N-850에 따라 진행되었으며, 접선전단하중에 대한 설계는 ASME BPVC III-2에 따라 수행되었다. 또한, 프리스트레스력을 설계하중이 아닌 휨인장강도의 일부로서 고려하여 휨과 축하중에 대한 설계 방법론을 확장시켰다.

매개변수 연구수행의 결과로, 우선 프리스트레스력을 하중 혹은 강도의 일부로서 고려하는 여부에 따라 P-M 상관도와 계수하중 사이의 양상이 달라지고, 그에 따라 배근양상이 달라짐을 확인할 수 있다. 콘크리트의 압축강도 개선은 주로 최대 허용 프리스트레스력을 증가시키는 데에서 이점을 보이며, 압축강도에 따른 철근량의 직접적인 감소량은 미미한 수준이다. 이에 반면, UHPC 적용시 인장강도 고려 여부에 따른 요구철근량은 직접적이고 유의미한 수준으로 감소되었다.

본 연구는 콘크리트 격납건물의 구상단계에서 인허가에 이르기까지의 광범위한 설계영역을 아우르지는 못하나, 그럼에도 매개변수 연구의 결과는 ASME 설계코드에 정립된 방법론을 따르는 동시에, 고성능 콘크리트의 특성과 요구철근량의 관계성에 대한 통찰을 제공할 수 있을 것으로 기대된다.

핵심용어: 콘크리트 격납건물, 고성능 콘크리트, 고강도 콘크리트, UHPC, 프리스트레스트 콘크리트, 설계코드, 극한강도설계법, P-M 상관도, 매개변수 연구
학번: 2020-27665